Research Article

Deep Learning-Based Active Jamming Suppression for Radar Main Lobe

Yilin Jiang ⓘ**, Yaozu Yang** ⓘ**, Wei Zhang** ⓘ**, and Limin Guo** ⓘ

College of Information and Communication Engineering, Harbin Engineering University, Harbin, China

Correspondence should be addressed to Yaozu Yang; yangyaozu@hrbeu.edu.cn

Due to the development of digital radio frequency memory (DRFM), active jamming against the main lobe of the radar has become mainstream in electronic warfare. The jamming infiltrates the radar receiver via the main lobe, covering up the target echo information. This greatly affects the detection, tracking, and localization of targets by radar. In this study, we consider jamming suppression based on the independence of RF features. First, two stacked sparse auto-encoders (SSAEs) are built to extract the RF characteristics and signal features carried out by the actual radar signal for subsequent jamming suppression. This method can effectively separate RF features from signal features, making the extracted RF features more efficient and accurate. Then, an SSAE-based jamming suppression auto-encoder (JSAE) is proposed; the mixed signal, including the radar signal, jamming signal, and noise, is input to JSAE for dimensionality reduction. Therefore, the radar signal and RF features, extracted by the two SSAEs in the previous step, are used to constrain the features of the reduced mixed signal. Moreover, we integrate the feature level and signal level to jointly achieve jamming suppression. The original radar signal is used to assist the radar signal reconstructed by the decoder. By first filtering out interference-related features and then reconstructing the signal, we can achieve better jamming suppression performance. Finally, the effectiveness of the proposed method is verified by simulating the actual collected data.

1. Introduction

The suppression of the radar main lobe active jamming has always been a key research issue in modern electronic warfare, especially after the wide application of digital radio frequency memory (DRFM) in the electronic countermeasures field that has greatly enriched the jamming mode; this resulted in higher demand on the antijamming capability of the radar. For instance, the intermittent sampling and forwarding jamming, generated by DRFM, can produce multiple false targets to overwhelm the real targets [1, 2]. The process of generating jamming by DRFM generally includes operations, such as intercepting radar signals, storing, sampling, or convolution and product operations with noise, and finally forwarding the processed jamming. Through this series of processing, the jamming, generated by the original radar signal, is strongly correlated [3]; therefore, extracting relevant signal features from the traditional time domain, frequency domain, or time–frequency domain has not led to effectively suppressing jamming.

Currently, algorithms for suppressing the new jamming types generated by DRFM are mainly designed from the system and system level, waveform design and receiver level, as well as signal and data processing level.

For instance, Guo et al. [4] proposed a method using independent component analysis (ICA) to suppress main lobe jamming. By utilizing principal component analysis (PCA) to extract the main lobe jamming component from the input mixed signal, separating the jamming samples in the time domain from the echo. A projection matrix was then created to suppress the main lobe jamming based on the separated samples. Cao et al. [5] utilized optimized quadrature phase encoding in transmit waveform design to mitigate interrupted sampling repeater jamming (ISRJ). The encoding objective function was derived from analyzing the principle of quadrature phase encoding against intermittent sampling jamming, followed by applying a genetic algorithm to determine the encoding sequence. In addition, Ly et al. [6] developed a CNN-based method for ISRJ identification and antijamming target detection. FrFT was applied to counter

SMSP jamming in distributed radar due to distinct FM slopes between spectrum dispersive jamming and radar signals [7]. Multiple studies [8–10] examined jamming suppression in distributed radar systems, identifying jamming signals by analyzing unique spatial scattering traits that differentiate genuine target echoes from deceptive jamming. Furthermore, Nie et al. [11] proposed a method, based on sub-pulse coding (SPC), to analyze single-channel synthetic aperture radar (SAR) systems against RF jamming (RFJ) and deception jamming (DJ). In addition, Tian et al. [12] proposed a scheme using mismatched filters to suppress chopping and interleaving (C&I) jamming by combining parameter estimation, signal reconstruction, and filter optimization based on enhanced time–frequency characteristics of the signal and jamming parameters. Furthermore, Li et al. [13] suggested a kurtosis-based algorithm to reconstruct SMSP jamming signals by determining the subpulse period, estimating the initial phase, and adjusting the amplitude through kurtosis maximization for effective signal suppression.

As a conclusion, the current study still has some limitations, almost all the abovementioned research results mainly focused on suppressing a certain main lobe active jamming. Therefore, facing the different jamming methods, it was necessary to reestimate the jamming parameters and design algorithms to extract several features. The deep neural networks (DNNs) can automatically mine and extract potential deep features; thus, using deep learning methods can generalize solutions to different jamming scenarios. On the other hand, the main lobe active jamming is generated by a jammer based on digital RF storage technology. Due to the nonlinearity of the frequency conversion link between the jammer, the RF power amplifier, and other devices, the introduced nonlinear distortion remodulates the modulated signal, and the resulting jamming signal becomes correlated with the RF signature of the jammer. Therefore, distinguishing jamming signals and radar signals from RF characteristics is of great significance to further suppress jamming. However, there is less open literature on the use of RF signatures to suppress radar jamming.

Thus, this paper proposes an algorithm to suppress different jamming patterns using stacked sparse auto-encoders (SSAEs) and RF characteristics. Moreover, the main contributions of this paper are summarized as follows:

(1) We propose two SSAEs to extract the RF characteristics. The signal, emitted by the source, contains both the signal features and the RF characteristics. If a single SSAE is applied, the extracted RF characteristics will be mixed with the signal features, resulting in a low integrity of the extracted RF characteristics. Therefore, two SSAEs models where one of them is employed to extract the signal features of the radar signal. These extracted signal features then serve as constraints, optimizing the other network to accurately and comprehensively extract RF characteristics.

(2) After extracting RF features by two SSAEs models, we verified the independence of RF features. This process allows confirming that the RF characteristics

of signals with different modulation methods emitted by the same source are identical. Moreover, we make sure that the RF characteristics of signals, having the same parameters and emitted by several sources, are different.

(3) We propose RF signatures combined with a jamming suppression auto-encoder (JSAE) to counter multiple main lobe active jammers. JSAE is mainly divided into two parts to suppress jamming: The first one consists of calling the signal features and RF characteristics of the radar signal that have been extracted in the encoding stage. Combining these two phases of features to form the feature labels yields to constrain the encoded features of the mixed signal. Given the autonomy of RF characteristics, the differences between the RF attributes of the jamming signal and the radar signal previously extracted by the two SSAE models become apparent. This divergence enables the identification and subsequent filtration of the jamming signal. As the signal characteristics within the feature label guide the filtration process, not only does it facilitate the elimination of the jamming signal; however, it also imparts constraints on the signal attributes within the composite signal. The second part is in the decoding stage, using the original radar signal to constrain the reconstructed signal output by the decoder.

Finally, the technical solution used in this paper is shown in Figure 1.

2. RF Signature for Jamming Suppression

In academia, there is no uniform definition of RF characteristics. Generally speaking, they are also known as unintentional modulation characteristics carried out by signals. Unlike intentionally designed modulation characteristics, unintentional modulation characteristics arise from the nonideal characteristics of hardware devices or characteristics or errors generated during the manufacturing process of the device. Therefore, RF characteristics are inherent properties of the physical level; they are independent, stable, and universal [14]. The first feature (i.e., independence) indicates that the RF characteristics, contained in each hardware device, are unique, while the second feature (i.e., stable) means that the RF characteristics will not change due to the external environment conditions. At present, RF signatures find widespread applications in wireless transmitter identification within the communication field and in individual radiation source identification in the radar field.

In this paper, both the radar signal and jamming signal are, respectively, simulated using the receiver to collect the signal data emitted by several signal source devices in the microwave anechoic room. Because of the nonideal characteristics of the internal semiconductor components of the hardware device, such as the signal source, the emitted signal will carry RF characteristics. Based on the RF characteristics of its own equipment, and knowing that both the radar signal and jamming signal are generated and transmitted by different types of signal sources, the RF characteristics carried by
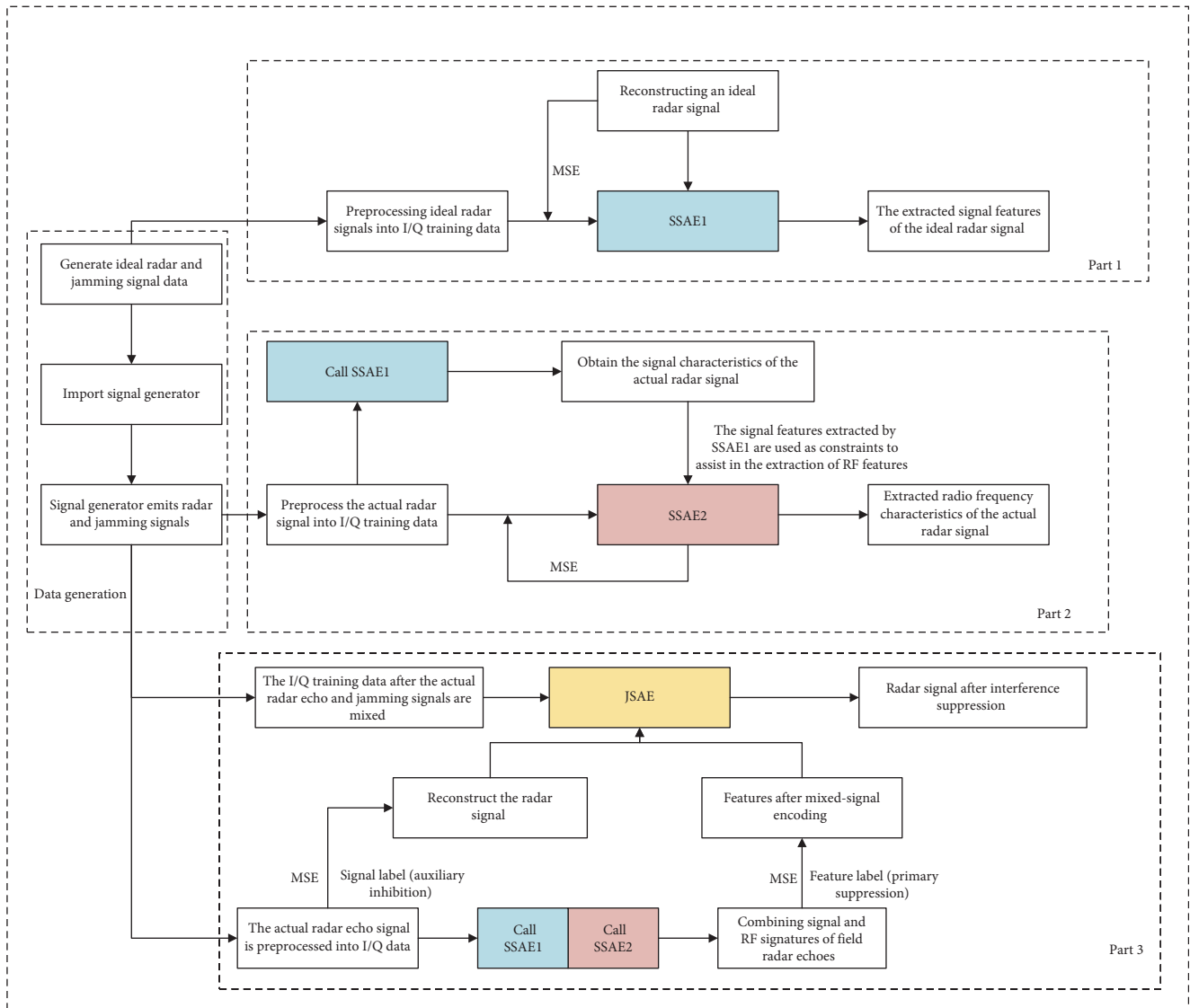
FIGURE 1: Overall schematic diagram.

the two types of signals are unique and stable. Therefore, the analysis of the jamming suppression is considered first. During this analysis, the RF characteristics, carried by radar signal and jamming signal, are independent; yet they have a corresponding relationship with the signal source equipment.

2.1. General Structure of Radar Transmitter. Currently, the main vibration amplification-type radar transmitter with the best performance is often used. The structure diagram of the overall components is shown in Figure 2. Although its composition structure is complex and its production cost is high, it is able to achieve the modulation of complex signals and generate coherent signals. The main vibration amplification-type radar transmitter consists mainly of a radiation source structure cascaded through a solid-state frequency source, a modulator, and an RF amplifier chain. The fundamental component of the solid-state frequency source is the frequency synthesizer. It is capable of producing RF signals with varying frequencies and modulation modes for the entire radar system. Moreover,

these frequencies sequentially traverse a three-stage amplification process within the RF amplification link to finally generate high-power RF signals. In the structure of the complete radar transmitter, due to the influence of the solid-state frequency source, the self-noise, and the nonlinear factors within the entire RF amplification link, the transmitted radar signal will carry out the RF characteristics. In addition, during the signal modulation process, it will introduce error; this error will be multiplied by the original signal and will introduce the RF characteristics to the signal.

2.2. DRFM Structure. The role of DRFM has grown substantially in contemporary electronic warfare. DRFM functions as an electronic mechanism for storing and retransmitting signals through high-speed digital acquisition technology. Moreover, DRFM [15] can store intricate modulated radar signal waveforms. In addition, the jamming signal, generated after processing, is highly similar to the original radar signal, resulting in high jamming performance and efficiency. The
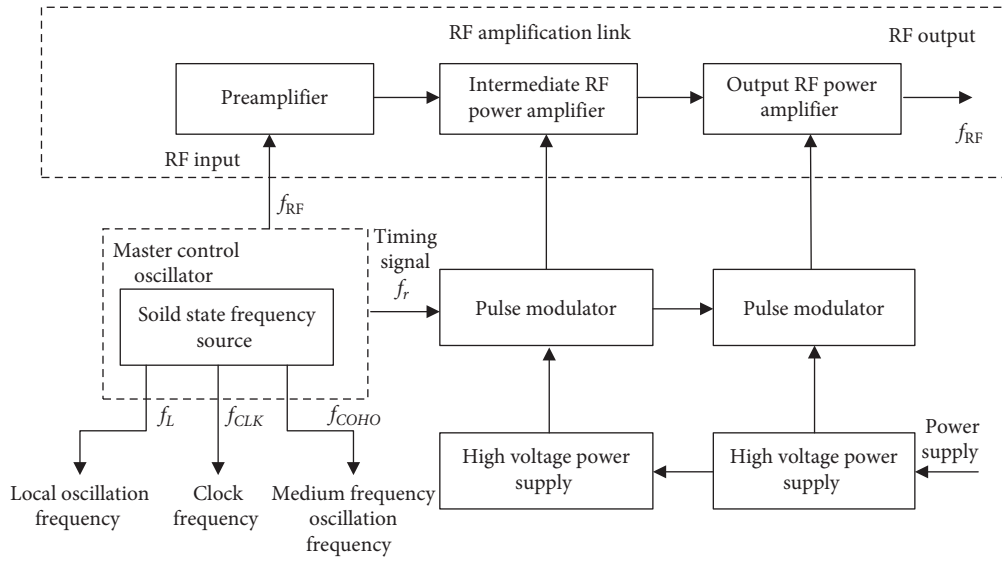
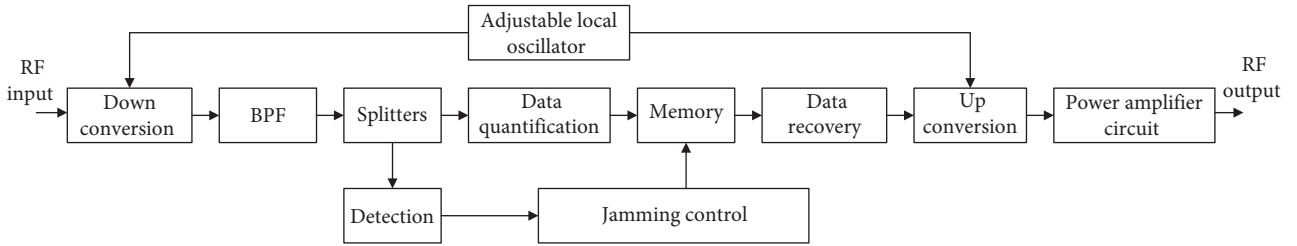FIGURE 2: Main vibration amplification type radar transmitter.

FIGURE 3: DRFM system circuit structure.

structure diagram of DRFM is displayed in Figure 3. Therefore, DRFM includes six components: down-conversion, data quantization, memory storage, number recovery, up-conversion, and jamming control.

During the generation of the jamming signal, the original radar signal is quantized by the analog-to-digital conversion, and the noisy signal is generated due to the quantization error. Concerning the digital-to-analog converter, it is used for data recovery as it forms flicker distortion due to the nonideal characteristics, and nonlinear distortion is generated by the power amplifier after up-conversion. The original input signal undergoes another modulation within each component of the jamming machine, resulting in forwarding jamming to generate spurious components, and noise in the jamming signal emitted. Thus, the jamming signal has RF characteristics.

3. Extraction of RF Features by Two SSAEs

DNNs are often used to extract data or images of hidden features [16, 17]. In this section, SSAE1 is the first method employed to extract the signal features from the ideal radar signal using unsupervised means. The ideal radar signal used is generated by simulation software without RF features. Then, SSAE1 is integrated with SSAE2 to form two SSAEs. These SSAEs are employed to extract the RF features of the real-pickup radar signal. The emitted signal by the signal

generator is referred to as the real-pickup signal in this paper. The use of two combined SSAEs leads to a better extraction of the RF features of the real-pick radar signal at different abstraction levels. This will ensure that the potential RF features of the signal generator, that can stably characterize the simulated radar radiation source, are identified based on the real-pick radar signal; moreover, the extracted RF features are not sensitive to signal parameter variations.

Since different signal generators are employed to simulate the radar side and the interferer side, respectively, the RF features, carried by the radar signal and the interferer signal collected at the receiver side, are different. This is used as the basis to achieve interference suppression. After the addition of noise to the mixed signal comprising both the radar signal and interferer signal as well as the input to JSAE, the primary focus in the interference suppression process is to impose constraints on the encoded mixed signal's features. These features are based on the RF features and signal features derived from the harvested radar signal. Moreover, they are extracted by the collaboration of the two SSAEs and are used as feature labels. Simultaneously, the original radar signal is utilized as signal labels to assist in constraining the reconstructed signal after decoding, under the two parts. Finally, the interference suppression is achieved by filtering out the interference signal and reconstructing the radar signal using the joint constraint of both parts.
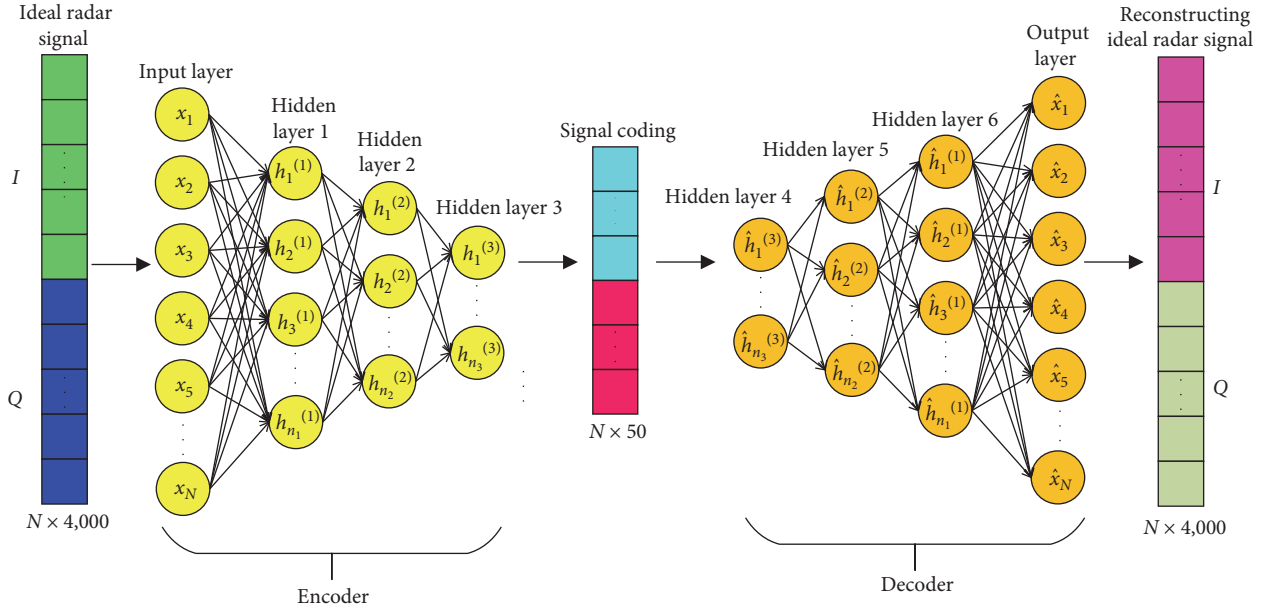
FIGURE 4: SSAE1 structure diagram.

3.1. Signal Feature Extraction by SSAE1.

The following steps are applied to extract the signal RF features of the ideal radar signal while using a single SSAE network. The SSAE is an unsupervised learning network model where the encoder and decoder are fully connected. Moreover, the SSAE is typically composed of multiple sparse auto-encoder (SAE) stacks, and a single SAE generally contains three layers: input, hidden, and output layers. Encoding occurs from the input to the hidden layer, whereas decoding is performed between the hidden to the output layer. Therefore, Figure 4 shows the SSAE1 structure for extracting the signal characteristics of the ideal radar signal. In more detail, the network structure consists mainly of an input layer, an output layer, a three-layer hidden layer serving as an encoder, and another three-layer hidden layer serving a decoder, with a fully connected structure between each layer.

Referring to Figure 4, three layers of SSAE1 are constructed with three encoders and decoders. Consequently, the dataset containing the ideal radar signal is normalized and inserted in SSAE1. In addition, the signal features of the ideal radar signal are extracted using the layered pretraining and global training fine-tuning. Finally, the SSAE1 model is saved after accomplishing the training. In this paper, all signal datasets, input to the network, are preprocessed to eliminate the real and imaginary components of the signal data. Subsequently, these datasets are connected to generate the in-phase and quadrature (I/Q) data. The input nodes of the neural network used in this paper consist of 4,000 samples.

In extracting the ideal radar signal features, the training process of SSAE1 follows the principle of layer-by-layer greedy training and supervised fine-tuning. First, the layer-by-layer training is applied to get the individual weights and biases of each layer. Then, these weights and biases serve as the initialization parameters of the whole deep-level network for global training, i.e., fine-tuning the whole network. Therefore, for the layer-by-layer pretraining, SSAE1 starts the self-encoding and training from the first layer, and the hidden features learned in the first AE layer will be used as input for the next AE layer. For example, after encoder1 has been trained using the first AE layer, the encoding phase is only left, and the output of the hidden layer of the first AE is used as the input layer of encoder2 of the second AE layer. Hence, auto-encoding and training are performed, and the parameters of the previous network layers remain stable. After the layer-by-layer training, the network is globally trained for fine-tuning. Thus, SSAE1 completes the signal feature extraction of the ideal radar signal by pretraining and fine-tuning.

If $\mathbf{X}$ is the unlabeled ideal radar signal input data, the output of layer i coding is represented as follows:

$$\mathbf{h}^i = f(\mathbf{z}^i) = f(\mathbf{w}^i\mathbf{h}^{i-1}+\mathbf{b}^i), \ 0 \leq i \leq n, \tag{1}$$

where $\mathbf{h}^i$, $\mathbf{w}^i$, and $\mathbf{b}^i$ are the activation vector, weight vector, and bias vector of layer i, respectively. Moreover, $\mathbf{z}^i = \mathbf{w}^i\mathbf{h}^{i-1} + \mathbf{b}^i$ denotes the excitation vector, and $f(\cdot)$ denotes the activation LeakyReLu function that is expressed as follows:

$$\text{LeakyReLu}(z) = \max(\alpha\mathbf{z}, \mathbf{z}), \tag{2}$$

where $0 < \alpha < 1$ is a preset parameter.

When $i = 0$, the input layer $\mathbf{h}^0 = \mathbf{X}$ represents the input of the network; however, when $i = n$, the network output layer is targeted, and the final linear output of the network $\mathbf{h}^n$ is the following:

$$\mathbf{h}^n = \mathbf{z}^n = \mathbf{w}^n\mathbf{h}^{n-1} + \mathbf{b}^n. \tag{3}$$

As already mentioned, SSAE1 is a three-layer codec network. A sparsity constraint is added to the hidden layer neurons
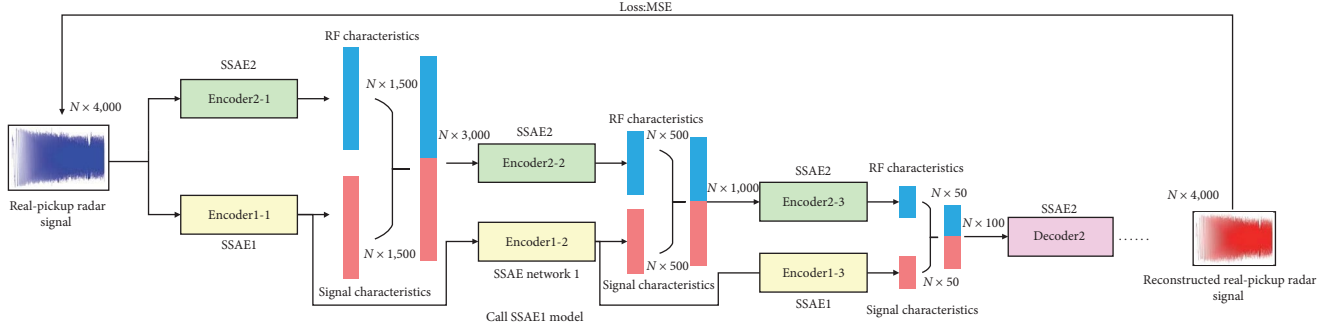
FIGURE 5: Flowchart of the two SSAEs for extracting RF features.

to ensure that the output of most neurons is null. Therefore, the network loss function of a single layer of SSAE1, during the pretraining phase, applies the mean squared deviation with the sparsity constraint term, as shown in the following equation:

$$\text{Loss}_1 = \frac{1}{N}\sum_{i=1}^{N}\frac{1}{2}\left\|\widehat{\mathbf{h}}_i - \mathbf{x}_i\right\|^2 + \beta\sum_{j=1}^{s_2}\text{KL}\left(\rho\,|\,\widehat{\rho}_j\right), \tag{4}$$

where N denotes the number of samples, $\mathbf{x}_i$ represents the ith sample of the single-layer encoder input in SSAE1, and $\widehat{\mathbf{h}}_i$ denotes the ith sample of the corresponding single-layer decoder reconstructed output. Moreover, S_2 represents the number of neurons in the hidden layer, ρ indicates the parameter of the sparsity constraint and it tends to zero, and $\widehat{\rho}_j$ is the average activation of the hidden neurons that is expressed as follows:

$$\widehat{\rho}_j = \frac{1}{N}\sum_{i=1}^{N}\left[a_j^{(2)}\left(\mathbf{X}^{(j)}\right)\right], \tag{5}$$

where $a_j^{(2)}\left(\mathbf{X}^{(j)}\right)$ denotes the activation of the hidden neuron j of the neural network with a network input $\mathbf{X}$. Since the hidden layer neuron should approach zero, it is necessary to control the value of $\widehat{\rho}$ by using ρ sparsity. Thus, the Kullback–Leibler (KL) divergence is constructed as a regular constraint term:

$$\text{KL}\left(\rho\,|\,\widehat{\rho}_j\right) = \rho\text{In}\left(\frac{\rho}{\widehat{\rho}_j}\right) + (1-\rho)\text{In}\left(\frac{1-\rho}{1-\widehat{\rho}_j}\right). \tag{6}$$

The β parameter in Equation (4) represents the weight of the control sparsity penalty factor with the following properties: when $\widehat{\rho}_j$ is close to zero or one, the relative entropy is large at this point; however, when $\widehat{\rho}_j$ is equal to ρ, $\text{KL}(\rho\,|\,\widehat{\rho}_j) = 0$ and it increases as the difference between $\widehat{\rho}_j$ and ρ becomes larger. Therefore, to satisfy the sparsity requirement, β should be minimized when $\widehat{\rho}_j$ is close to ρ [18–23]. Moreover, the pretraining to extract the signal characteristics of the ideal radar signal is conducted by minimizing the mean square error (MSE) between the estimated values of the decoded layers and the input values of the encoded layers to get the initial values of the parameters and update them. This provides the basis of the global training to fine-tune the parameters.

After pretraining and fine-tuning, the parameters for the global training, the following loss function, that deploys the MSE criterion, is applied:

$$\text{Loss}_1 = \frac{1}{N}\sum_{i=1}^{N}\|\widehat{\mathbf{y}}_i - \mathbf{y}_i|^2, \tag{7}$$

where $\mathbf{y}_i$ denotes the ith ideal radar signal input, and $\widehat{\mathbf{y}}_i$ is the ith reconstructed ideal radar signal, obtained from the last layer of the decoder output. Fine-tuning the parameters during global training serves to optimize the parameters and update the network. This is achieved by the minimization of the MSE between the reconstructed signal and the ideal radar signal.

3.2. Two SSAEs to Extract RF Features. After applying SSAE1 and extracting the signal features from the ideal radar signal, three SAEs are employed to construct the three-layer SSAE2 to extract the RF features. The structure of SSAE2 is identical to SSAE1. Therefore, it contains an input layer, an output layer, a three-layer hidden layer serving as an encoder, and a three-layer hidden layer serving as a decoder. The original radar signal dataset is normalized and inserted into the SSAE2 to extract the RF features through hierarchical pretraining, global training, and fine-tuning. Since the radar signal input to the SSAE2 contains signal features and RF features, the former area extracted by SSAE1 and must be used as constraints to optimize the extraction of RF features by SSAE2 to ensure the complete and accurate extraction of these features. The flowchart of the two SSAEs for extracting RF features is displayed in Figure 5.

The layer-by-layer pretraining and global training differ between SSAE2 and SSAE1. The second layer of the SSAE2 encoder input represents the combined output from the previous layer of the SSAE1 and SSAE2 encoders, and the combined output contains the first layer of the SSAE1 encoder output. The combined output of the second-layer encoder of SSAE2 is input to the second-layer decoder of SSAE2 for reconstruction, and the MSE of the encoder input of the second-layer of SSAE2 is calculated. As previously presented, both SSAE1 and SSAE2 have three encoding layers. The layer-by-layer pretraining ends when SSAE2 is combined
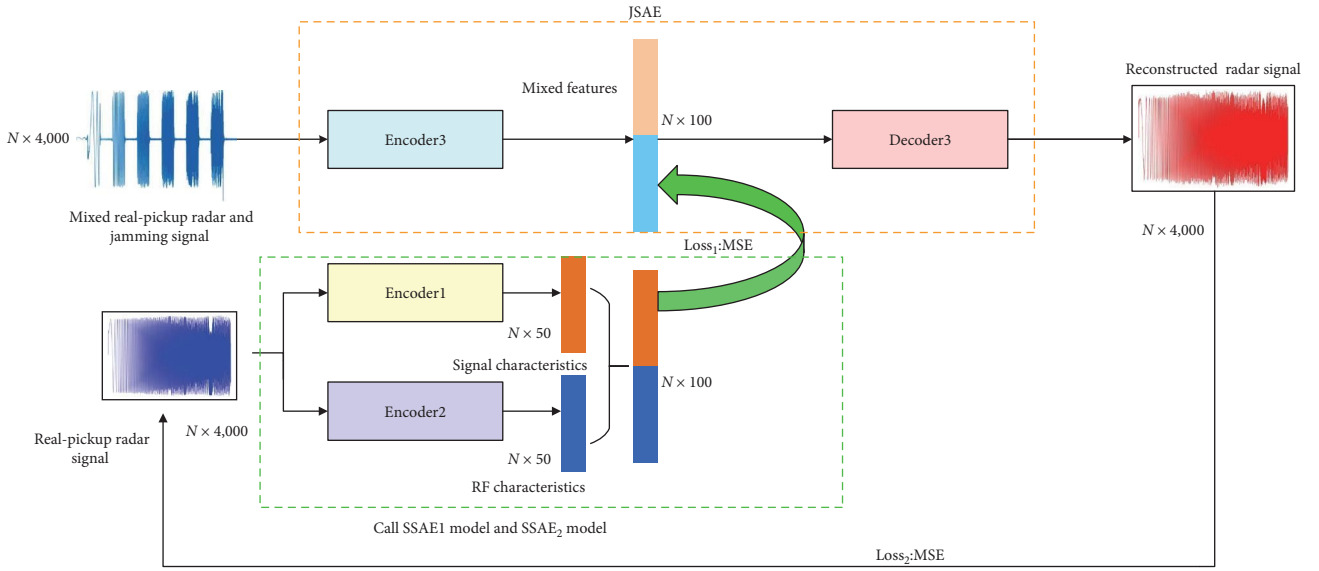
FIGURE 6: JSAE training process.

with SSAE1 to complete the third layer of SSAE2 encoding and decoding training. In the layer-by-layer pretraining, the decoder output of SSAE2 and the encoder input of each layer calculate the MSE and are used to initialize and update the network parameters of that layer. Moreover, the loss function of the SSAE2 layer-by-layer training is identical to the SSAE1 layer-by-layer training, and the sparse constraint term, defined in Equation (4), is applied.

Subsequently, the global training of SSAE2 is conducted to fine-tune the network parameters. The first-layer coding outputs of SSAE2 and SSAE1 are merged and input into the second-layer encoder of SSAE2. Then, the second-layer coding outputs of SSAE2 and SSAE1 are merged and input into the third-layer coding of SSAE2. The coded output of the third layer of SSAE2 represents the RF characteristics. The third-layer coding outputs of SSAE2 and SSAE1 are merged and input into the third-layer decoder for reconstruction. The network parameters of SSAE2 are updated by calculating the MSE using the reconstructed signal from the last layer of the encoder and the original input signal. The loss function of SSAE2 for global training and fine-tuning is equivalent to that of SSAE1 for global training (Equation (7)).

4. JSAE Jamming Suppression

4.1. Primary and Secondary Suppression. Two different signal sources are used to simulate the radar transmitter and the jammer because the two signal generators, considered in this study, are different. Thus, the radar signal emitted by the source and the simulated signal have distinct RF features, providing a basis for jamming suppression. The network structure of JSAE is identical to SSAE1 and SSAE2. Moreover, jamming suppression is performed using the feature level as the primary part and the signal level as the secondary part. First, the RF features of the real radar signal are extracted by both SSAEs, and the signal features are considered as feature labels to restrict the hybrid features obtained using

layer-by-layer coding of the mixed signal consisting of the radar signal and the interference signal generated by JSAE. Then, the mixed features are decoded layer-by-layer by JSAE to get the reconstructed radar signal. Finally, the real radar signal is employed as the signal label to constrain the reconstructed radar signal. Note that the JSAE training process is shown in Figure 6.

The RF characteristics and signal characteristics of the extracted radar signals, as depicted in Figure 6, serve as encoding filters. The use of the extracted RF characteristics of the radar signals helps distinguishing between radar signals and interference signals within mixed signals, thereby suppressing interference.

Moreover, the use of the extracted signal characteristics of the radar signals provides a foundation for subsequent signal reconstruction. The mixed signals consist of both RF characteristics and signal characteristics carried out by the interference signals as well as the radar signals. This implies that the mixed signals contain a combination of both types of characteristics. Leveraging the unique and constant nature of RF characteristics, the extracted RF features from radar signals are used to constrain the mixed features following JSAE multilayer encoding. This differentiation enables discrimination between the RF characteristics of the radar signals and interference signals within the mixed signals, thereby achieving interference suppression. While using the extracted RF characteristics of the radar signals for interference suppression, concurrent employment of the extracted signal characteristics from these radar signals is applied to enhance the constrain on mixed features following the encoding. Then, the filtering stage of the signal characteristics, related to interference signals from the mixed signals, results in more accurate signal characteristics of the radar signals. Note that the precise signal characteristics are crucial for reconstructing radar signals. Interference suppression is initially executed at the feature level, using both the RF features and signal features from the extracted radar signal. These features

are employed to constrain the hybrid features obtained after encoding the hybrid signal. Subsequently, the hybrid features derived from the compression of the hybrid signal are decoded and recovered layer-by-layer by JSAE to obtain the reconstructed radar signal. Finally, the original radar signal is used to enhance the reconstructed radar signal after carrying out suppression at the signal level. As for the second interference suppression, it is performed at the signal level. In other words, JSAE uses the RF features, signal features, and the signal itself to complete the interference suppression; however, the interference suppression from the feature level is primary, and the suppression at the signal level serves only as an aid to the interference suppression at the feature level. Therefore, this suppression is secondary. Finally, the primary and secondary are considered by setting the weight coefficients of the loss function.

4.2. Pretraining and Global Training of JSAE. The JSAE training also consists of layer-by-layer pretraining and global training, but these two parts differ from those of the first two networks (e.g., SSAE1 and SSAE2). JSAE only uses the feature labels to enhance the mixed features after each encoding layer; therefore, it does not decode and reconstruct the features after each layer. During global training, JSAE uses the feature labels and signal labels to limit the features after three layers of encoding and decodes the reconstructed signals. The first layer-by-layer pretraining step consists of inserting the mixed signal composed of the radar signal with the target and the jamming signal to serve as the training set. This set will be used later on to train JSAE. The completed SSAE1 and SSAE2 are meanwhile used. The mixed signal is coded in the first layer to obtain the mixed features containing the RF and signal features. The real radar signal is input into SSAE1 and SSAE2. After the first-layer coding of both networks, the signal and RF features of the first layer are obtained separately. Then, both parts of features serve as feature labels and are jointly substituted into the loss function along with the encoded features of the mixed signal to calculate the MSE. Furthermore, the JSAE layer-by-layer training loss function includes a sparse constraint term to extract deep-level features. The expression of the loss function in the hierarchical pretraining can be expressed as follows:

$$\text{Loss}_2 = \frac{1}{N} \sum_{j=1}^{N} \frac{1}{2} ||\widehat{\mathbf{h}}_j - \mathbf{h}_j||^2 + \beta \sum_{j=1}^{s_2} \text{KL}(\rho || \widehat{\rho}_j), \quad (8)$$

where $\widehat{\mathbf{h}}_j$ denotes the output feature of the jth mixed signal passing through the single-layer encoder of JSAE, and $\mathbf{h}_j$ denotes the ith feature label.

In addition, the layer-by-layer greedy training mode is applied. The input of the encoder in the second layer of JSAE training is the output of the first-layer encoder. Thus, the input of the second-layer encoder represents the hybrid feature output of the first-layer encoder. The hybrid feature is then encoded using the second-layer encoder that generates a hybrid feature with fewer dimensions. Similar to the first-layer training, real radar signal features, encoded by the second layer of SSAE1, and RF features, encoded by the second

layer of SSAE2, are combined to form the feature tags. Moreover, the MSE between the combined feature labels and the mixed features of the mixed signal, derived from the second-layer encoding of JSAE, is calculated. By analogy, the pretraining of JSAE third layer is completed.

Subsequently, global training is performed to update the network parameters. Thus, the mixed signal is fed into JSAE to be hierarchically encoded, and the final dimension-reduced mixed features are obtained from the output of the third encoding layer. Although the mixed signal undergoes three-layer encoding for dimension reduction, the actual radar signals are processed through the three encoding layers of SSAE1 to get the signal features of the final dimension-reduced radar signal. Additionally, the actual radar signals are also processed through the three encoding layers of SSAE2 to generate the RF features of the final dimension-reduced radar signal. These two feature parts are then merged and used as feature labels. The first term of the loss function for global training is calculated by computing the MSE value between the feature labels and the mixed features obtained from the three-layer encoding of JSAE. The dimension-reduced mixed features are then decoded through the three JSAE decoding layers to reconstruct the radar signal. Subsequently, the actual radar signals are used as signal labels, and their MSE, with the reconstructed radar signals, is considered as the second term of the loss function. The main difference between the global training and the layer-wise training of JSAE is that, during global training, only the mixed features obtained from the third layer are used to determine the value of MSE with the merged feature labels; moreover, the MSE is computed between the decoded reconstructed radar signals and the original radar signals. Thus, the expression for the loss function of JSAE global training is determined as follows:

$$\text{Loss}_2 = \lambda_1 \times \frac{1}{N} \sum_{k=1}^{N} \left\| \widehat{\mathbf{h}}_k - \mathbf{h}_k \right\|^2 + \lambda_2 \times \frac{1}{N} \sum_{i=1}^{N} \|\widehat{\mathbf{y}}_i - \mathbf{y}_i\|^2,$$

$$(9)$$

where $\mathbf{h}_k$ represents the signal features and RF features output from the combined kth real radar signal after the third layer of SSAE1 and SSAE2 coding, $\widehat{\mathbf{h}}_k$ denotes the mixed features obtained from the kth mixed signal after the third layer of JSAE coding, and λ_1 and λ_2 denote the weight coefficients of both mean squared deviations in the loss function, respectively. Note that $\lambda_1 > \lambda_2$ as JSAE performs jamming suppression primarily at the feature level and aids in constraining the jamming at the signal level. During training, we explored various combinations of weighting parameters while ensuring that $\lambda_1 > \lambda_2$ and $\lambda_1 + \lambda_2 = 1$. The specific values of λ_1 and λ_2 have a negligible impact on the final results; therefore, they do not significantly affect the overall jamming suppression performance.

5. Analysis of Experimental Results

5.1. Experimental Data Setup. An ideal radar signal, required for extracting signal features using simulation software, is first generated. This signal includes two modulation signals

commonly used in pulsed radar systems, the linear frequency modulation (LFM) and the binary phase-shift keying (BPSK). To avoid overfitting, since the same signal data are input into SSAE1, a small amount of Gaussian white noise is added to the ideal radar signal, yielding to a signal-to-noise ratio (SNR) equal to 30 dB. The real radar signal used for RF feature extraction and jamming suppression consists also of these two modulation methods. Since the signal features extracted by SSAE1 in applied to assist SSAE2 in RF feature extraction, the signal parameters of the collected radar signal shall be maintained constant as the ideal radar signal. The ideal signal data of the baseband, generated by the simulation platform, are sent to the signal generator, which modulates the baseband signal into an RF signal. Then, the RF signal is transmitted by the signal generator, and the final collection is the I/Q data of the zero intermediate frequency signal; this latter is obtained after the received signal undergoes down-conversion and filtering processing by the receiver.

In more detail, Table 1 lists the parameters of the ideal radar signal generated by the simulation platform and the ones emitted by the signal generator. This represents the input data for SSAE1 and SSAE2. Moreover, different transmit power levels and carrier frequencies are used for the RF signal emitted from the signal source. The data generation and acquisition of the jamming signal are the identical to the radar signal. Therefore, the signal generator processes the jamming signal data, generated by the simulation platform, and emits the jamming RF signal, which is received and processed by the receiver. Five different jamming signals with distinct jamming styles are used at this level. They have a jamming-to-signal ratio (JSR) range of 10–30 dB. Moreover, the parameters of the jamming signals are listed in Table 2. Finally, the network parameters of SSAE1 for signal feature extraction, SSAE2 for RF feature extraction, and JSAE for jamming suppression are displayed in Table 3.

The reason for setting the number of network layers to three in both SSAE1 and SSAE2 is to efficiently extract radio frequency features and signal features without prolonging the training time. Reducing the number of layers to two would affect the extraction of radio frequency features, consequently influencing the jamming suppression performance. Moreover, opting for a four-layer network during training would yield to limited feature extraction effects but significantly increase the iteration time. To maintain compatibility with JSAE, which relies on features extracted from the networks SSAE1 and SSAE2, these latter are configured with three layers. JSAE needs to use the features extracted by the first two networks, so it also needs to maintain the three-layer network settings. In addition, the number of nodes in each layer of the networks is reasonably determined based on the signal length. Therefore, the node settings for the input layer and each encoding layer need not adhere strictly to the manuscript's specifications; they can be adjusted according to the actual signal characteristics.

Floating points of operations (FLOPs) represent the number of floating point operations and are employed to measure the computational effort of the model. Subsequently, we assess the computational complexity of the model based on FLOPs.

Moreover, SSAE1, SSAE2, and JSAE all incorporate a fully connected structure. The number of parameters and computational performance (FLOPs) of the fully connected layer are computed using the following equations:

$$\text{Params} = \left(N_{\text{input}} + 1\right) \cdot N_{\text{output}}, \tag{10}$$

$$\text{FLOPs} = 2 \cdot N_{\text{input}} \cdot N_{\text{output}}, \tag{11}$$

where N_{input} and N_{output} represent the number of input and output nodes of the fully connected layer. Table 4 shows the number of parameters and FLOPs for each network.

5.2. Signal Data Acquisition. The radar transmitter and jammer are simulated using transmitting and receiving equipment in a microwave anechoic chamber. Moreover, the radar and jamming signal data are collected to analyze the RF characteristics of the different signal sources. The schematic diagram of the transmitting and receiving equipment is shown in Figure 7.

The signal sources deployed at the transmitting end are Keysight N5172B and Keysight N5182B. Both signal generators are RF vector signal generators. Finally, the Ceyear 4051E signal/spectrum analyzer is used as the receiver end.

We chose LFM and BPSK signals as the radar signal. As the jamming signal, ISRJ, SMSP jamming, C&I jamming, smart noise convolution jamming, and smart noise product jamming were applied. Keysight N5172B was used to simulate the radar signal transmission for the two different modulation methods, and Keysight N5182B was applied to compute the signal transmission of the five types of jamming patterns. In addition, this second tool has another purpose. It was used to simulate and transmit the radar signals keeping the same signal parameters and modulation parameters as Keysight N5172B. After that, by extracting and comparing the RF features of both tools, it can be verified that the signals with the same parameters and modulation methods, and emitted by different signal sources, contain different RF characteristics.

We denote the transmitted LFM signal as $s(t)$:

$$s(t) = \text{Arect}\left(\frac{t}{T}\right)\exp\left\{j2\pi\left(f_c t + \frac{1}{2}Kt^2\right) + j\varphi_0\right\}, \tag{12}$$

where A is the amplitude of the signal, T represents the pulse width of the signal, f_c denotes the carrier frequency of the signal, and φ_0 is the initial phase, which is null; moreover, $K = \frac{B}{T}$ is the FM slope, and B is the bandwidth of the signal. Referring to Equation (10), the rectangular pulse $\text{rect}(t)$ is represented as follows:

$$\text{Rect}\left(\frac{t}{T}\right) = \begin{cases} 1, & -\dfrac{T}{2} \le t \le \dfrac{T}{2} \\ 0, & t > \dfrac{T}{2}, t < -\dfrac{T}{2} \end{cases}. \tag{13}$$

A 7-bit Barker code sequence was applied for encoding. The BPSK is expressed as follows:

TABLE 1: Parameters of radar signal.

Structure	Modulation method	$\varphi(t)$	f_c (GHz)	B (MHz)	T (μs)	Transmit power, P (dBm)	Barker code $m(t)$	Code width (μs)
Ideal signal	LFM	$2\pi f_c t + K\pi t^2$	0	20	40	—	—	—
	BPSK	$2\pi f_c t + \pi m(t)$	0	—	40	—	$[-1\ -1\ -1\ 1$ $1\ -1\ 1]$	5.7
Actual radar signal	LFM	$2\pi f_c t + K\pi t^2$	1–3	20	40	10–30	—	—
	BPSK	$2\pi f_c t + \pi m(t)$	1–3	—	40	10–30	$[-1\ -1\ -1\ 1$ $1\ -1\ 1]$	5.7

TABLE 2: Signal parameters of the jamming signal at the transmitter.

Jamming patterns	Jamming parameters		SNR
Smart noise convolution jamming	Noise time width, L_s (μs)	20, 30, 40	
Smart noise product jamming	Noise bandwidth, B_s (MHz)	3, 4, 5	
SMSP jamming	Sampling multiplier, N	4, 5, 8	JSR: 10–30 dB
	Number of segments of signal interception, m	3, 4	
C&I jamming	Number of copies per subpulse, n	2, 3	
ISRJ	Number of intervals for sampling, M	3, 4, 5	

TABLE 3: Parameter setting of the networks.

	SSAE1	SSAE2	JSAE
Parameters		Value	
Input layer	4,000	4,000	4,000
Hidden layer 1	1,500	1,500	3,000
Hidden layer 2	500	500	1,000
Hidden layer 3	50	50	100
Hidden layer 4	500	1,000	1,000
Hidden layer 5	1,500	3,000	3,000
Output layer	4,000	4,000	4,000
Learning rate	0.0001	0.0001	0.0001
Optimizer	Adam optimizer	Adam optimizer	Adam optimizer
Activation function	LeakyReLU	LeakyReLU	LeakyReLU

TABLE 4: Number of parameters and flops.

Neural network	Params	FLOPs
SSAE1	13.56M	27.10M
SSAE2	36.22M	72.40M
JSAE	66.43M	132.80M
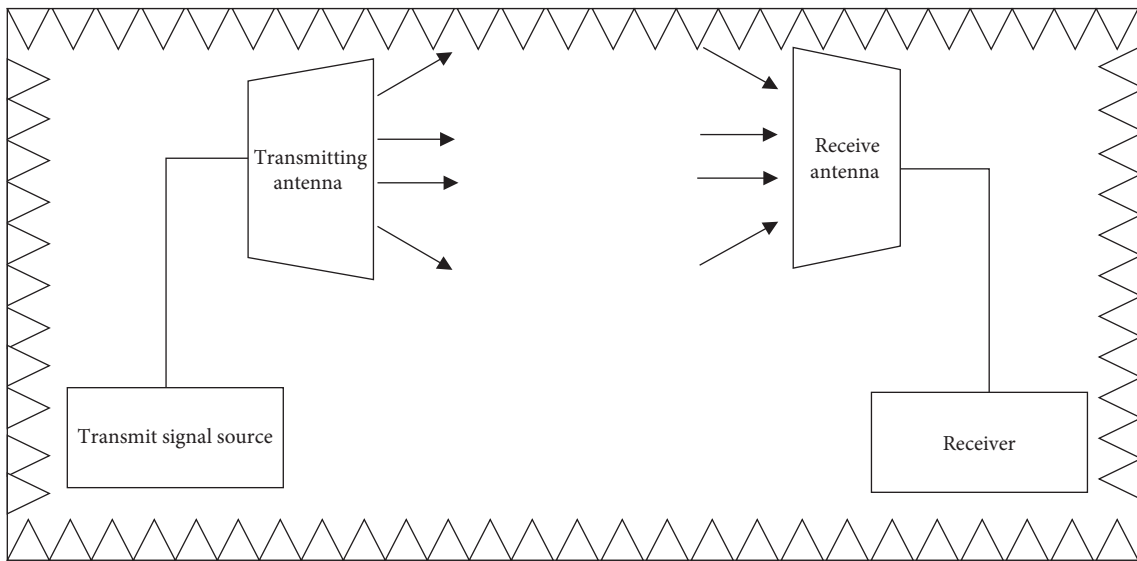
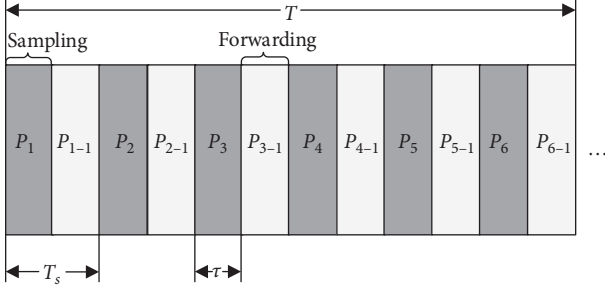FIGURE 7: Schematic diagram of the transmitting and receiving equipment.

FIGURE 8: Schematic diagram of ISRJ.

FIGURE 9: Schematic diagram of C&I jamming principle.

$$s(t) = A\operatorname{rect}\left(\frac{t}{T}\right)\exp\{j[2\pi f_c t + \phi(t) + \varphi_0]\}, \tag{14}$$

where $\phi(t)$ represents the phase modulation function ($\phi(t) = \pi m(t)$), and $m(t)$ indicates the 7-bit Barker code sequences. As the value of $m(t)$ is either 0 or 1, the value of $\phi(t)$ will be 0 or π.

The principle of ISRJ generation consists of intercepting the radar signal by the jammer antenna, storing it, sampling it, and forwarding it. Sampling and forwarding actions are performed sequentially until the end of the signal [24]. In more detail, the schematic diagram of ISRJ is shown in Figure 8, where T_s represents the sample plus one period of intermittent forwarding, and τ indicates the sample period. Therefore, the sampling signal is defined as follows:

$$
\begin{aligned}
p(t) &= \operatorname{Rect}\left(\frac{t}{\tau}\right) \times \sum_{n=-\infty}^{+\infty} \delta(t - nT_s) \\
&= \frac{\tau_j}{T_s} + \frac{2\tau}{T_s}\sum_{n=1}^{+\infty}\frac{\sin n\pi f_{st}\tau_j}{n\pi f_{st}\tau_j}\cos 2\pi n f_{st}t, \ 0 < t \le T,
\end{aligned} \tag{15}
$$

where $f_{st} = \frac{1}{T_s}$ is the frequency of the ISRJ. The model of ISRJ is defined when the radar signal is expressed with respect to $s(t)$ as indicated below:

$$
\begin{aligned}
J_3(t) &= s(t) \cdot p(t) \\
&= \frac{\tau_j}{T_s}s(t) + \frac{2\tau_j}{T_s}\sum_{n=1}^{+\infty}\frac{\sin n\pi f_{st}\tau_j}{n\pi f_{st}\tau_j}\cos 2\pi n f_{st}t \cdot s(t), \ 0 < t \le T.
\end{aligned} \tag{16}
$$

Moreover, SMSP jamming exhibits a high overlap in the time and frequency domains of radar echoes. For instance, Sparrow et al. [25] observed several comb-like dense false targets after pulse compression that reduces the radar detection performance [26]. SMSP jamming consists of multiple subpulses, which are sampled and reconstructed by DRFM after intercepting the radar signal. If there are n subpulses of SMSP jamming and the FM slope of the jamming $k = nK$, the signal model of the ith subpulse can be expressed as follows:
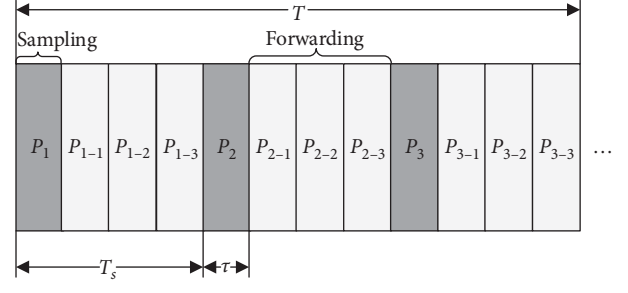
$$
\begin{aligned}
j_i(t) &= \operatorname{Rect}\left(\frac{t - (2i - 1)T/(2n)}{T/n}\right) \\
&= \operatorname{Exp}\{j2\pi f_c[t - (i - 1)T/n] + j\pi nK[t - (i - 1)T/n]^2 + j\varphi_j\},
\end{aligned} \tag{17}
$$

where φ_j is the initial phase of the jth subpulse. The reconstructed amplitude normalized SMSP jamming signal model is expressed as follows:

$$J_2(t) = \sum_{i=1}^{n} j_i(t). \tag{18}$$

In addition, C&I jamming is another type proposed by Sparrow et al. [25]. A high-density false target group is formed after matching the filtering. Moreover, C&I jamming differs from SMSP jamming in that the FM slope of the subsignal is identical to that of the intercepted radar signal. Therefore, C&I jamming can be regarded as the result of superimposing the ISRJ after applying multiple time delays [27, 28]. The principle of C&I jamming is displayed in Figure 9. This type consists of repeatedly applying Equation (14). Finally, the signal model of C&I jamming is expressed as follows:

$$J_3(t) = \sum_{n=0}^{N-1} J_1(t - n\tau). \tag{19}$$

In smart noise convolution jamming, the jammer receives the radar signal and performs a convolution modulation on both the noise and the radar transmission signal. Thus, the signal is amplified and transmitted [29]. The jammer receives the radar signal with a time delay τ; moreover, the Gaussian white noise generated by the jammer is presented by $n_1(t)$. The signal model of the smart noise convolution jamming is expressed as follows:

$$J_4(t) = s(t - \tau) \otimes n_1(t), \tag{20}$$

where $\otimes$ denotes the convolution operation.

Similarly, in smart noise product jamming, the radar transmits the signal, and the noise signal is multiplied, modulated, and amplified to be ready for transmission. In contrast to smart noise convolution jamming, the noise signal is a Gaussian white noise after applying the low-pass filtering [30, 31].

The signal model of the smart product jamming noise signal is expressed as follows:

$$J_5(t) = s(t - \tau) \times n_2(t). \tag{21}$$

In Equation (18), $n_2(t)$ is a narrowband noise signal and can be expressed as a low-pass filtering operation of $n_1(t)$ as indicated in the following equation:

$$n_2(t) = n_1(t) \times H(t). \tag{22}$$

Furthermore, the Ceyear 4051E signal/spectrum analyzer is deployed as the receiver for RF signals. The receiver's sampling rate is specified to be 1.25 times the measurement bandwidth on this device. In addition, after down-conversion processing, the receiver takes a low-pass filtering operation on the received RF signals setting the measurement bandwidth at the receiver side as the bandwidth of the low-pass filter. Therefore, attempting to further increase the sampling rate of the signal at the receiver end, it is required to artificially increase the measurement bandwidth; however, this approach can make the signal more spurious and seriously distorted. Thus, it will not be used for subsequent research, by testing and observing the time domain and frequency domain waveforms of the acquired signal. So, it can be concluded that the measurement bandwidth is optimal when it is equal to twice the bandwidth of the transmitted signal.

Therefore, we have selected the following parameter values, taking into account both the number of input nodes of the neural network and the limitations of the receiver equipment. These parameters are the bandwidth of the fixed transmitter jamming signal and radar signal that is set to 20 MHz, the sampling rate of the fixed transmitter baseband signal and the receiver sampling rate of the signal that is equal to 50 MHz, and the pulse width of the signal that is equal to 40 μs.

The ideal radar signals of each of the two modulation methods are generated using the simulation software with 4,750 sets consisting of the dataset of SSAE1. The N5172B signal generator is used to transmit both LFM and BPSK signals, encompassing various combinations of transmit power and distinct carrier frequencies. According to Table 1, five sets of transmit power levels and carrier frequencies are configured for the transmitted signals. Hence, when considering free combination, there are 25 different transmit power and carrier frequencies for each modulation mode of radar signals that are transmitted at the transmitting end. These signals, coming from the two modulations, are collected by the receiver side and regrouped in 190 groups for each combination of transmit power and carrier frequency; therefore, a total of 4,750 groups are considered for each modulation under 25 combinations of parameters, and a total of 9,500 groups are obtained for both modulations; they constitute the dataset of SSAE2. As for the N5182B signal generator, it also transmits five types of jamming signals. Table 2 shows that the signal parameters are adjusted for each type of jamming signal, so that each one has three different signal parameters. Consequently, when being merged with the combination

of different transmit power and carrier frequency parameters, the N5182B will transmit 75 different transmit power, carrier frequency, and jamming signal parameters for each type of jamming. The receiver side collects 16 sets for each combination of parameters; thus, a total of 1,200 sets are collected for each type of jamming, resulting in a total of 6,000 sets of data for the five types of jamming. Then, the different values of the dry signal ratio for each type of jamming are set as shown in Table 2.

In addition, since the RF features are only related to the hardware devices, another 6,000 sets of LFM signals are deployed, serving as radar echoes generated by N5172B. The signal parameters of the radar echoes are identical to those of the LFM signals in the dataset used to extract the RF features, i.e., 240 sets are used for each parameter combining the different transmit power and carrier frequencies. The 6,000 sets of LFM signals are combined with another 6,000 sets of jamming signals collected by N5182B. Moreover, different noise levels are added, and the mixed signals are utilized as the training and test sets for JSAE, while the LFM signals, obtained separately, are used for the JSAE tagging dataset.

Finally, the neural networks used in this study are trained using the minimum mean square error (MMSE) criterion to optimize the loss function and evaluate the performance of the network models. The dataset for each neural network is randomly divided: it consists of 80% of the input dataset for the training, while the remaining 20% is used for testing purposes.

5.3. Simulation Process.
The simulation platform is based on Python 3.8 and Tensorflow—Gpu, whereas the Spyder platform is used for debugging.

5.3.1. Data Generation and Acquisition.
The simulation software is used to generate the ideal radar signal for both modulation methods (Table 1). The ideal radar signal is generated by the N5172B signal generator, and the receiver gets the RF radar signal. The RF feature extraction is performed. Finally, the N5182B is used to transmit both modulation types with the same signal parameters as the N5172B radar signal and is acquired by the receiver. The signal is used for the RF feature comparison. As for the LFM signal, it is transmitted through the N5172B and acquired at the receiver side as the radar echo. Different types of interference signals are generated using the simulation software and transmitted through the N5182B signal generator. Finally, the acquired radar echoes are combined with different interfering signals, resulting in mixed signals.

5.3.2. Establish the Dataset.
The real and imaginary parts of the complex signal data, obtained in Step 1, are extracted and combined, i.e., the first half of each sample data is the real part, whereas the second half represents the imaginary part. The data are normalized and divided into a training set and a test set for each network dataset.

5.3.3. Establish the Neural Network.
SSAE1, SSAE2, and JSAE are built according to the structure shown in Figures 4–6, as well as Table 3, respectively.
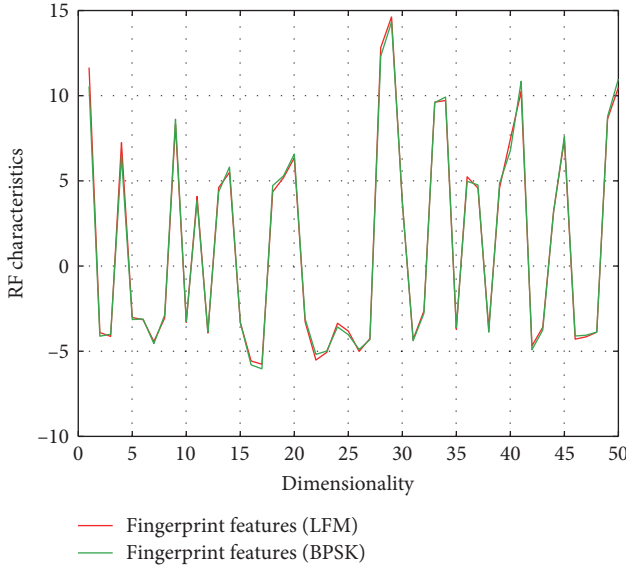
FIGURE 10: RF features extracted from different modulated signals (N5172B).

FIGURE 11: RF features extracted from different modulated signals (N5182B).

5.3.4. Extraction Characteristics. SSAE1 extracts the signal features from the ideal signal and the RF features from the radar signal transmitted by N5172B. Moreover, SSAE2 extracts the RF features from the radar signal transmitted by N5182B. The results of both parts of the RF features are compared. Furthermore, a comparison is proposed between the RF features contained in radar signals of different modulation methods emitted by the same signal generator. This is achieved to verify the independence of the RF features; therefore, the RF features exhibit a mapping relationship with the individual hardware and are independent of the signals themselves.

5.3.5. Jamming Suppression. The signal and RF features of the radar signals, emitted by the N5172B signal generator and extracted in step 4, are used as feature labels to participate in the JSAE training. Moreover, the radar signals, generated by the N5172B and acquired by the receiver, are utilized as signal labels to participate in the JSAE training to achieve jamming suppression.

5.3.6. Test Suppression Effect. The test set is used to verify the performance of the trained JSAE model on the reconstructed radar signal after jamming suppression. The algorithm's ability to suppress jamming is evaluated through pulse compression of the suppressed reconstructed signal and a comparison of the SNR gain curves before and after suppression.

5.4. Simulation Results and Discussion. Figures 10 and 11 show the 50-dimensional RF features extracted from the signals generated by N5172B and N5182B, respectively, for the different modulation methods. Moreover, Figures 12 and 13 show a comparison of the reconstructed and the original signals generated by N5172B and N5182B, respectively.

Furthermore, the RF features extracted from different modulated signals, emitted by the same signal generator, remain consistent. This verifies that the RF features remain unchanged across different signal parameters and are exclusively linked to
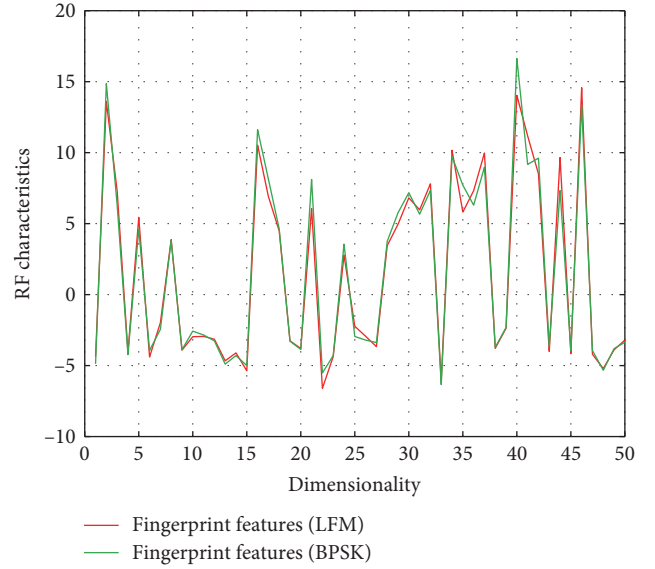
the hardware device. However, the RF features, extracted from signals emitted by different signal generators with the same parameters, are not consistent, indicating that the RF features have unique characteristics. The decoder reconstructs the signal by retrieving the feature information that was initially extracted by the encoder in the layers; thus, the comprehensiveness and accuracy of feature extraction are critical in the process of signal recovery. The recovered LFM and BPSK signals show that the reconstructed signal overlaps with the original input signal, indicating good reconstruction performance by both SSAEs.

The signal data $r(t)$ of JSAE's training set consists of three parts: the collected LFM echo signal $s(t)$ emitted by N5172B, the jamming signal $j(t)$ emitted by N5182B, and the Gaussian white noise $n(t)$ with an SNR varying between −10 and 30 dB. These are fed into the JSAE network for training; therefore, the expression is as follows:

$$r(t) = s(t) + j(t) + n(t). \tag{23}$$

The JSAE undergoes pretraining and global training, following Equation (9), with feature labels serving as the primary constraint and signal labels serving as the auxiliary constraint. After finishing the training phase, the JSAE model is saved, and the performance of jamming suppression is evaluated by applying the test set. Therefore, Figures 14(a)–18(a) show the pulse pressure before and after applying the jamming suppression for the five jamming types where JSR and SNR are equal to 30 dB. Moreover, Figures 14(b)–18(b) show the comparison between the reconstructed signal and the original signal after suppression.

The pulse pressure map, prior to suppression, shows that the primary lobe of the pulse compression, generated by the real target signal, is almost completely obscured by the dense false target spikes. This concealment effectively masks
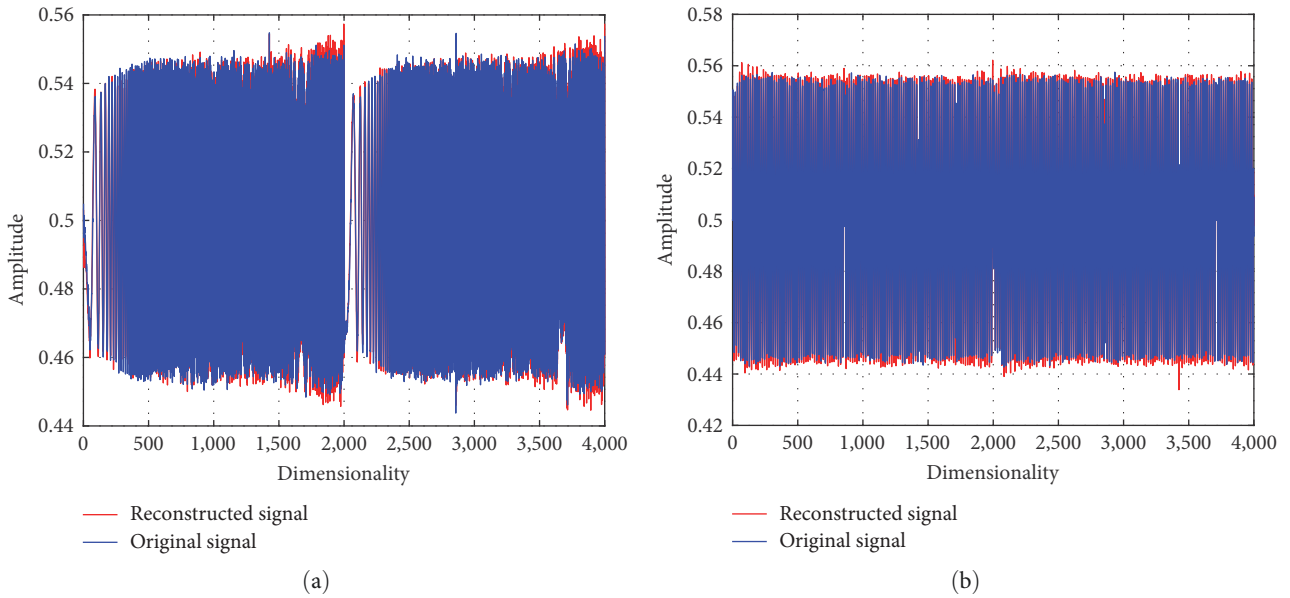
FIGURE 12: Comparison of reconstructed and original signals (N5172B): (a) LFM and (b) BPSK.
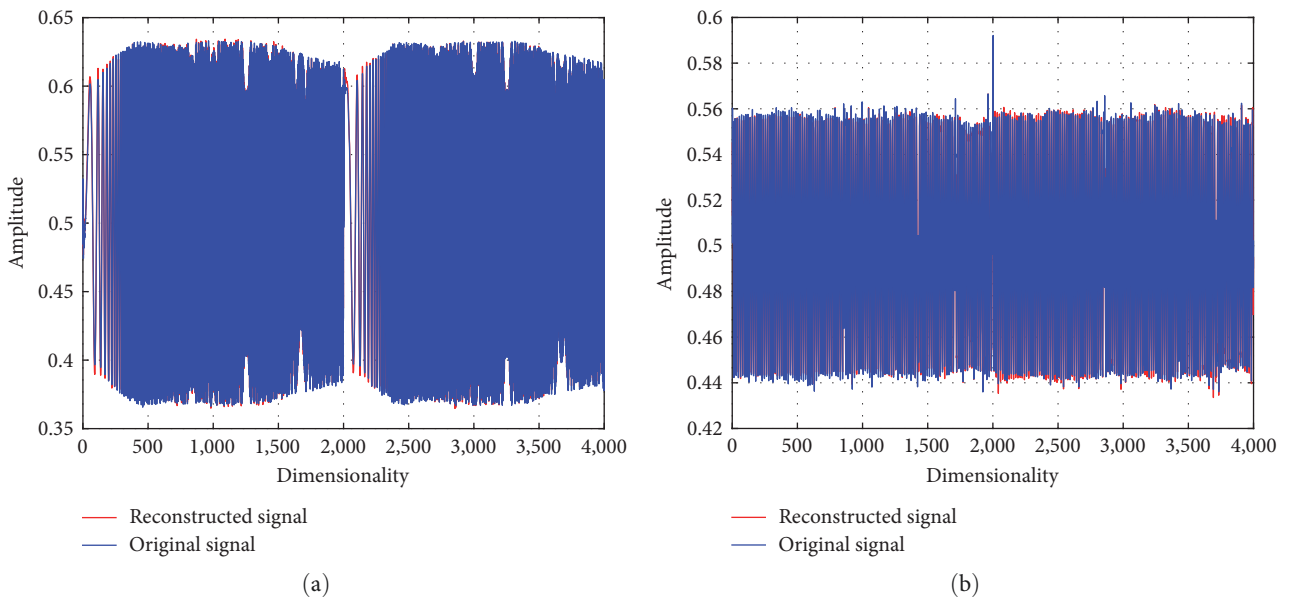

FIGURE 13: Comparison of reconstructed and original signals (N5182B): (a) LFM and (b) BPSK.

the real target and poses significant challenges for radar detection. The suppressed pulse pressure map can obviously get the location of the target pulse pressure spikes more accurately by filtering out the false target spikes caused by the jamming signal via pulse compression. However, the pulse pressure spikes of the suppressed signal can coincide well with the pulse pressure spikes without interference. This shows that the spikes, generated by the mixed signal after suppression and then through the pulse pressure, are the real target. Forwarding the false target signals so that the generated false target amplitude is reduced by more than 20 dB. After the elimination of the smart noise interference, the

target peak can be accurately detected and the side lobe of the pulse pressure will be reduced by more than 15 dB.

The comparison of the reconstructed and original signals revealed that the first three jamming types provide reconstructed signals identical to the original signal. However, the last two jamming types generate lower jamming suppression performance due to the different jamming mechanisms. Therefore, smart noise jamming is generated by adding noise and the intercepted radar signal through convolution or multiplication modulation. The first three types of sample-and-forward jamming only involve the sampling and retransmission of the intercepted radar signal without incorporating secondary
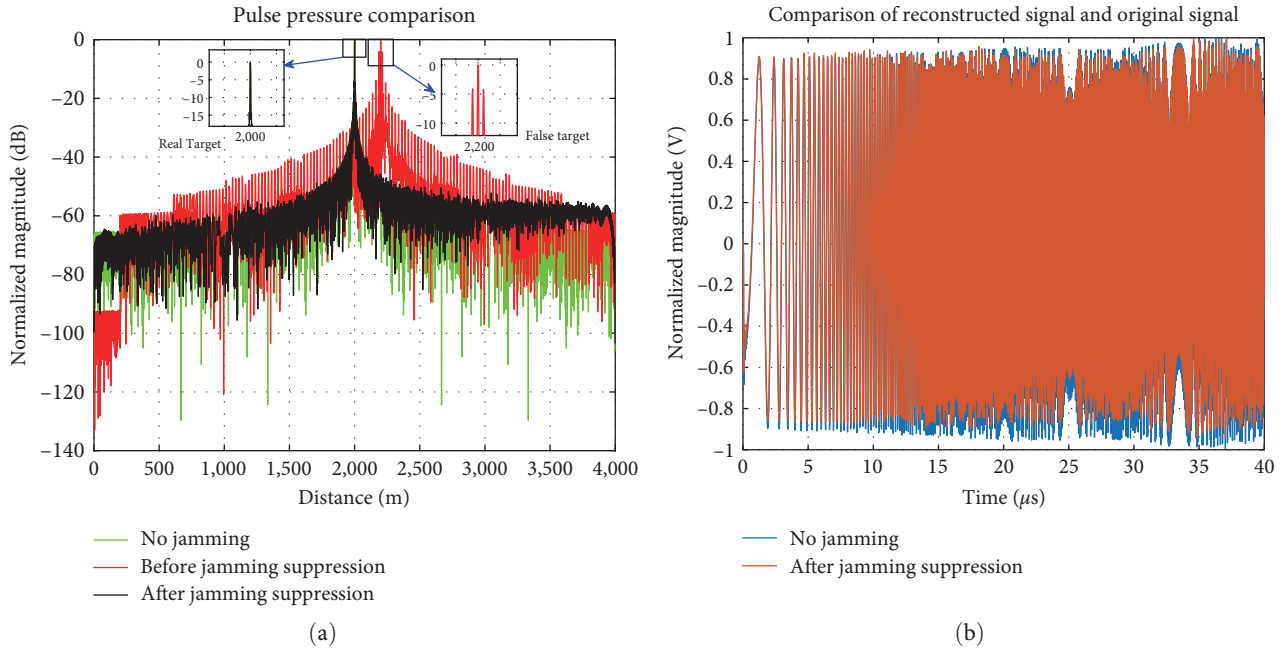
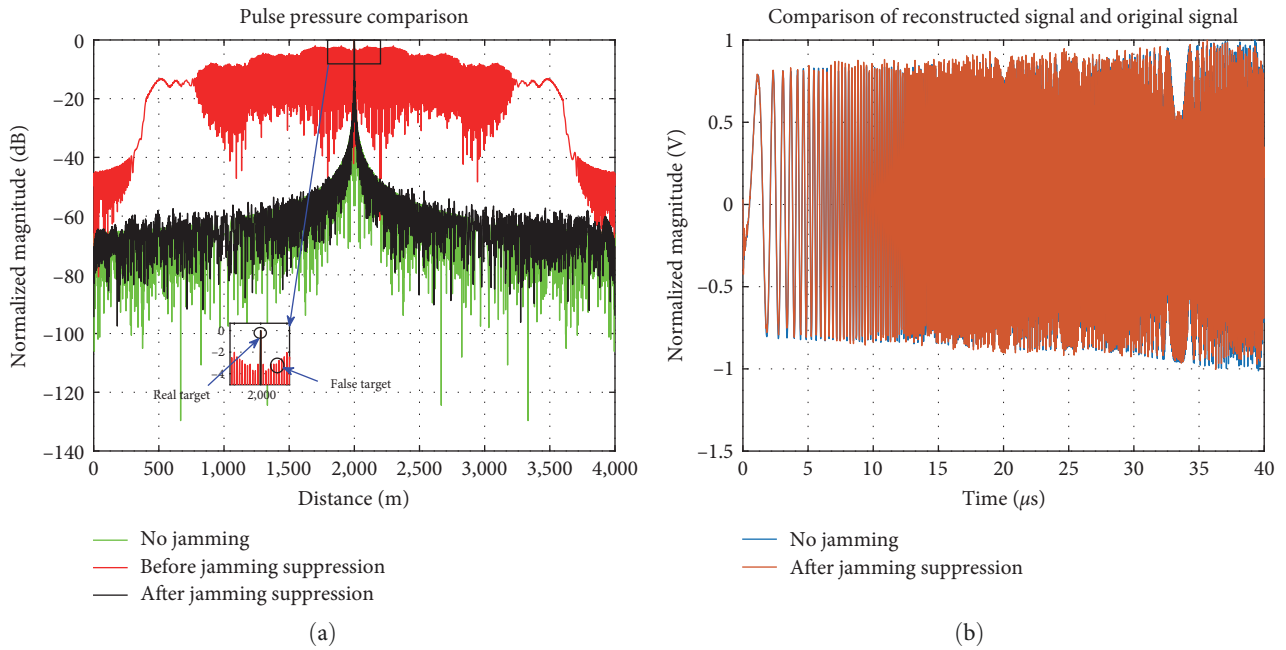Figure 14: (a, b) Interrupted sampling repeater jamming.

Figure 15: (a, b) SMSP jamming.

modulation with noise. Although there is a difference in the accuracy of the reconstructed signals after interference suppression between forwarding jamming and smart noise jamming, the JSAE suppression is able to eliminate false targets and accurately get the location of the real target, verifying the excellent performance of the proposed method.

We carried out a quantitative analysis of the jamming suppression performance using this method. The SINR gain is R where $R = \text{SINR}_2 - \text{SINR}_1$. Moreover, SINR_1 represents the signal-to-jamming and the noise ratio before jamming suppression, whereas SINR_2 indicates the signal-to-jamming and noise ratio after jamming suppression. Furthermore, Figure 19(a)–19(e) shows the results for SNR varying between −10 and 30 dB for the five jamming types. Referring to these findings, R increases with the JSR. If the JSR is high, the accuracy of applying combined features to filter out the
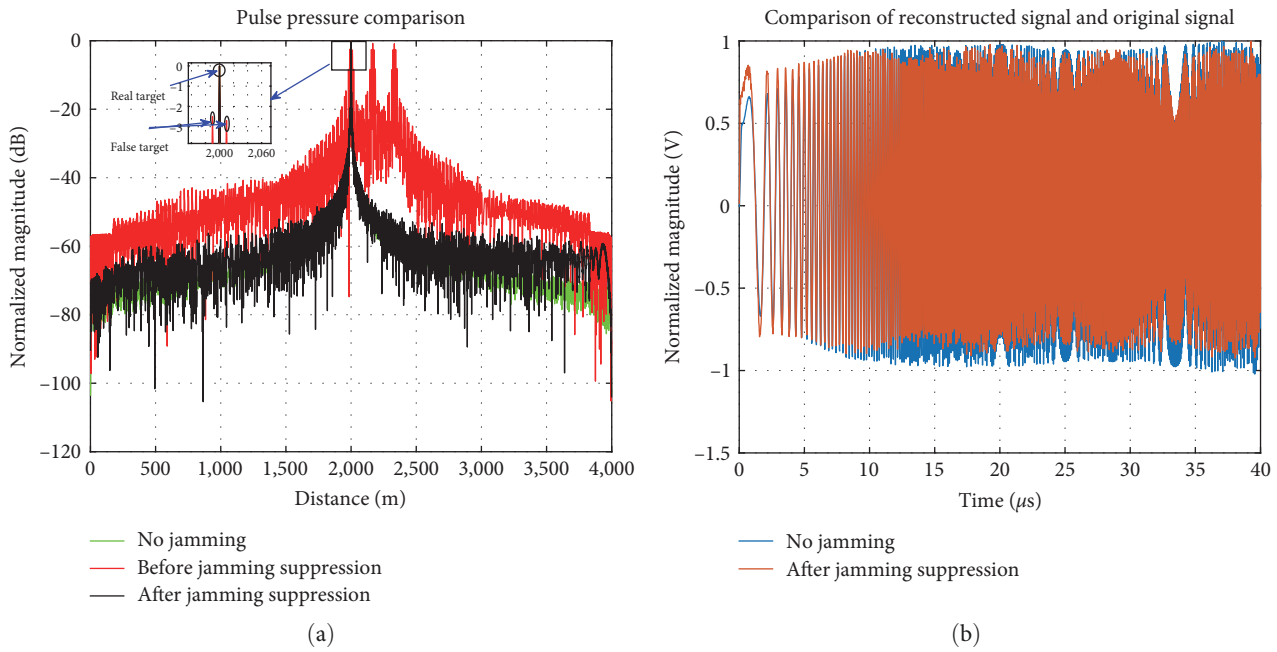
(a)

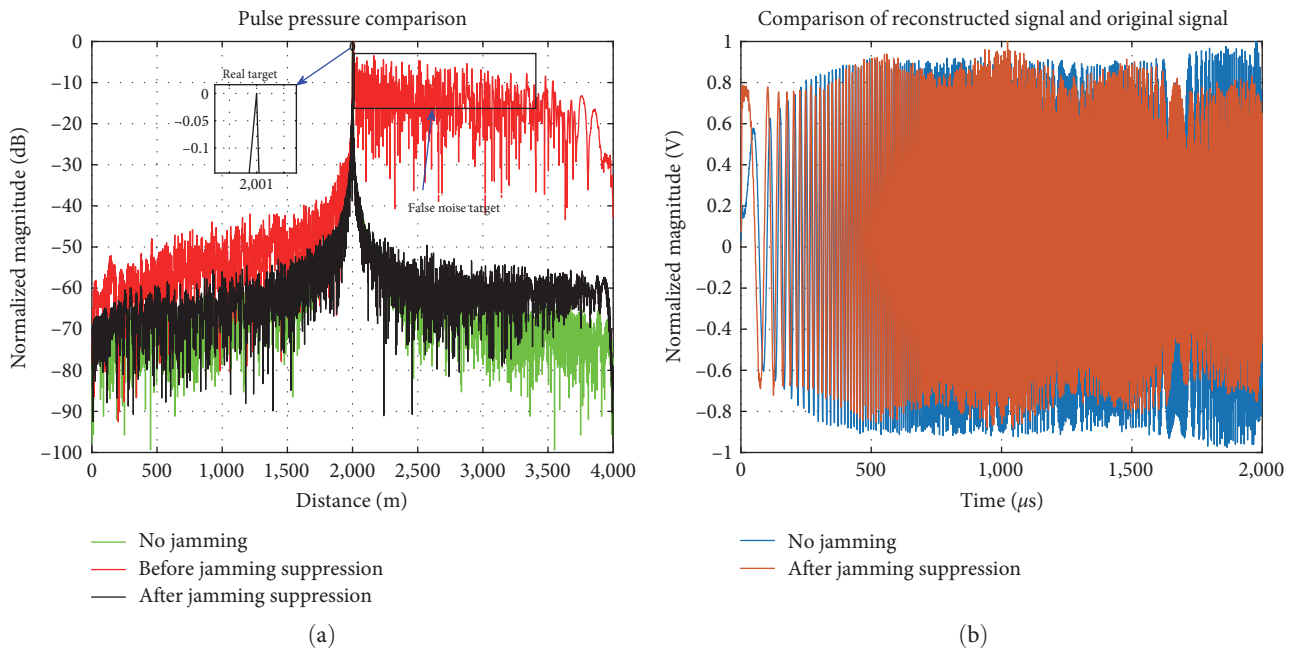(b)

FIGURE 16: (a, b) C&I jamming.

(a)

(b)

FIGURE 17: (a, b) Smart noise convolution jamming.

jamming signal and reconstruct the radar signal after distinguishing the jamming signal and radar signal with RF features is higher, resulting in better jamming suppression performance.

Since there is no existing literature regarding the suppression of multiple interferences using DNNs, the comparison experiment in this paper is determined to quantitatively compare the SMSP jamming suppression algorithm proposed by Li et al. [13] with the JSAE suppression of SMSP jamming. Therefore, Figure 20 shows the comparison of the

signal-to-jamming and noise ratio gain curves of the algorithm proposed in this paper against the SMSP jamming suppression algorithm outlined in Li et al.'s [13] study, under various SNRs.

First, we compare the influence of SNR. The results indicate that the SNR has a clearer effect on the suppressing SMSP jamming algorithm proposed in Li et al.'s [13] study compared to the proposed method in this work. Comparing the SINR gain changes in the two stages of SNR = −10∼20 dB and
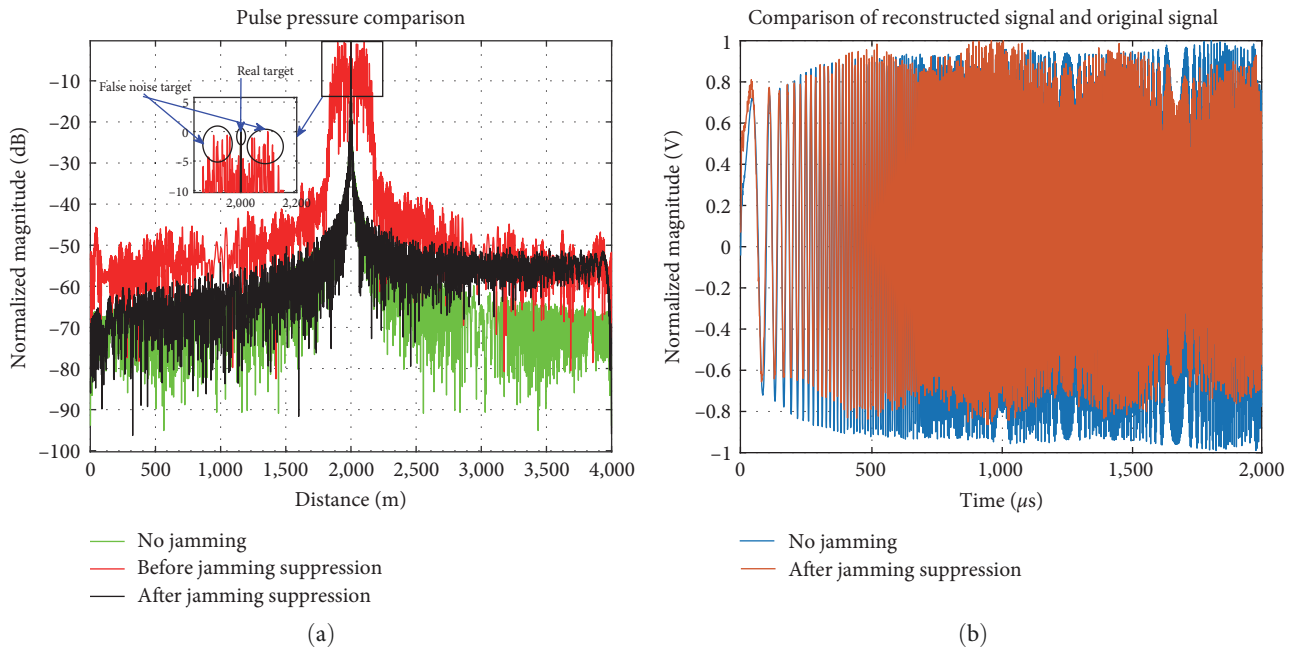
(a)

(b)

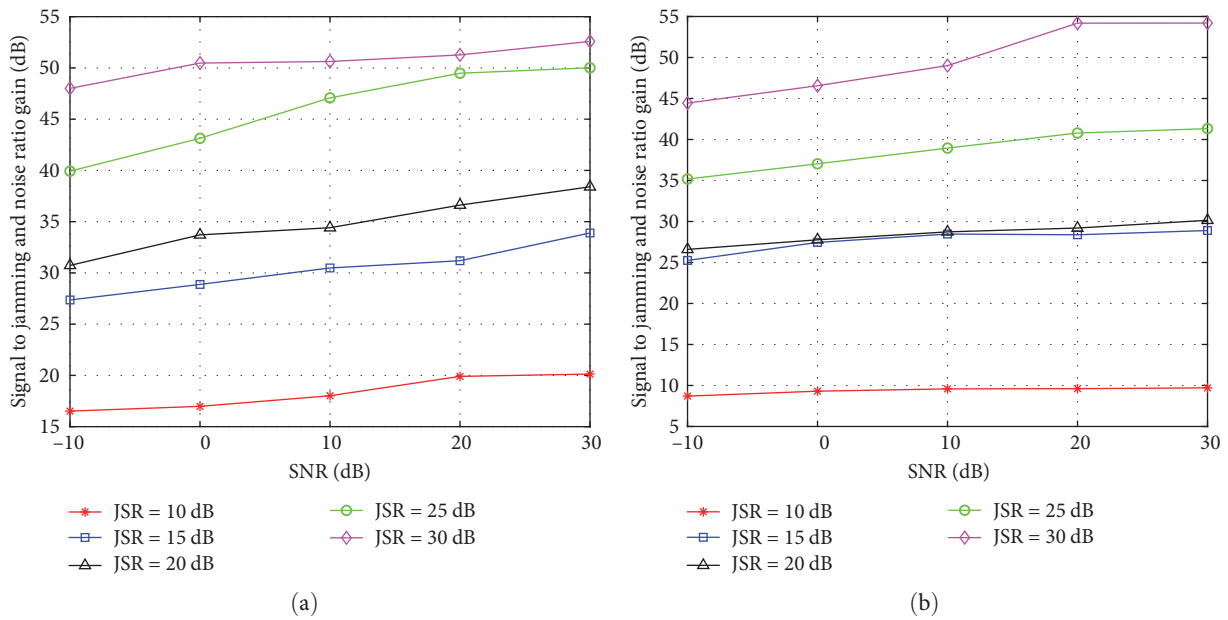FIGURE 18: (a, b) Smart noise product jamming.
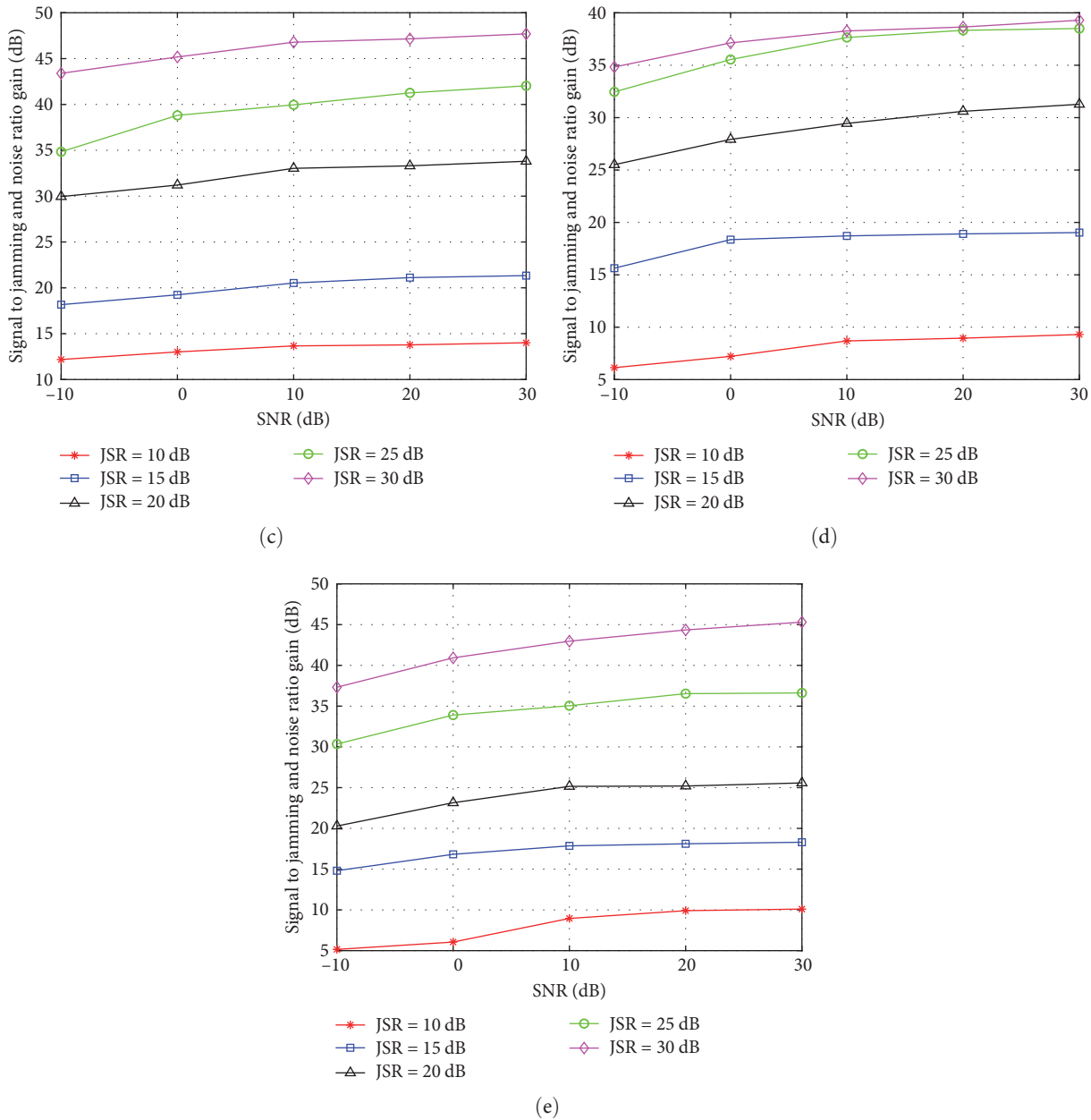

(a)

(b)

FIGURE 19: Continued.

FIGURE 19: SINR gain after jamming suppression for (a) ISRJ, (b) SMSP jamming, (c) C&I jamming, (d) smart noise convolution jamming, and (e) smart noise product jamming.

SNR = 20 dN~30 dB, following the SNR conditions of the previous stage, the SINR gain curve increases more rapidly; therefore, the SINR gain curve rises more rapidly at high SNR. However, there is a significant difference in the ability to obtain the SINR gain under low SNR conditions. However, after suppressing the SMSP interference in this paper, the SNR gain curve rises at both SNR stages (SNR = −10~20 dB and SNR = 20~30 dB). The increase is relatively gentle and there is no big gap, so the algorithm proposed in this paper is less affected by SNR.

Then, a comparison between the SINR gains obtained by the two methods under different JSR conditions is performed. For a low JSR, such as JSR = 10 dB, the SINR gain, obtained by the algorithm proposed in this paper, is better under low SNR conditions [13]. Conversely, when SNR is high, the algorithm in Li et al.'s [13] study demonstrates a larger SINR gain; however, in actual situations, the value of JSR is usually higher than 10 dB. Under this consideration, the SINR gain, obtained after SMSP interference suppression, is obviously better than the algorithm proposed in Li et al.'s [13] study. In addition, the interference suppression algorithm proposed in this paper can effectively figure against a variety of interferences, not just one interference suppression. Therefore, under comprehensive comparison, JSAE has better generalization ability, high efficiency, and robustness.
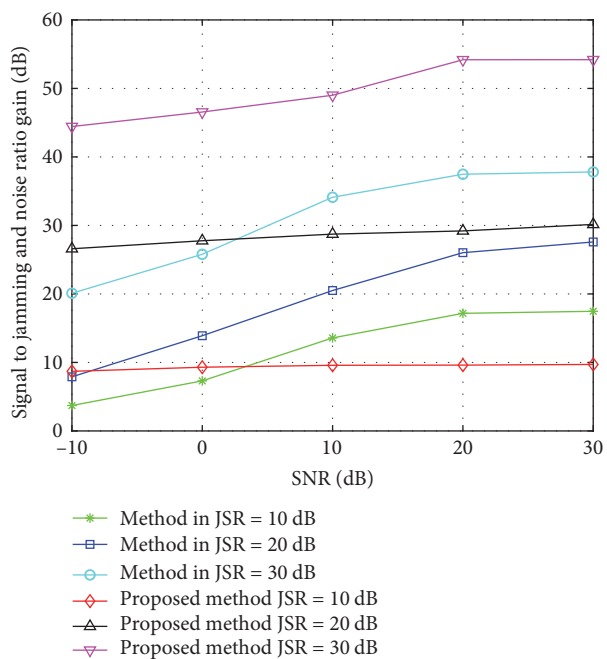
FIGURE 20: Comparison of the SINR gain after suppressing SMSP interference for the proposed method and the method in Li et al.'s [13] study.
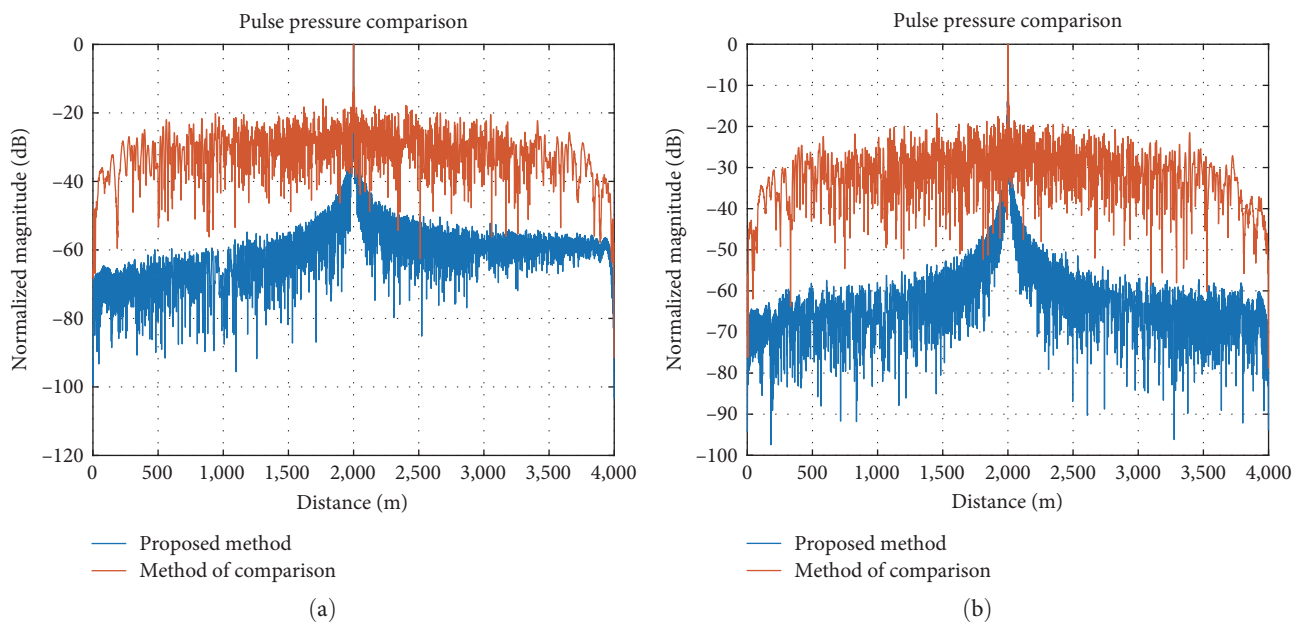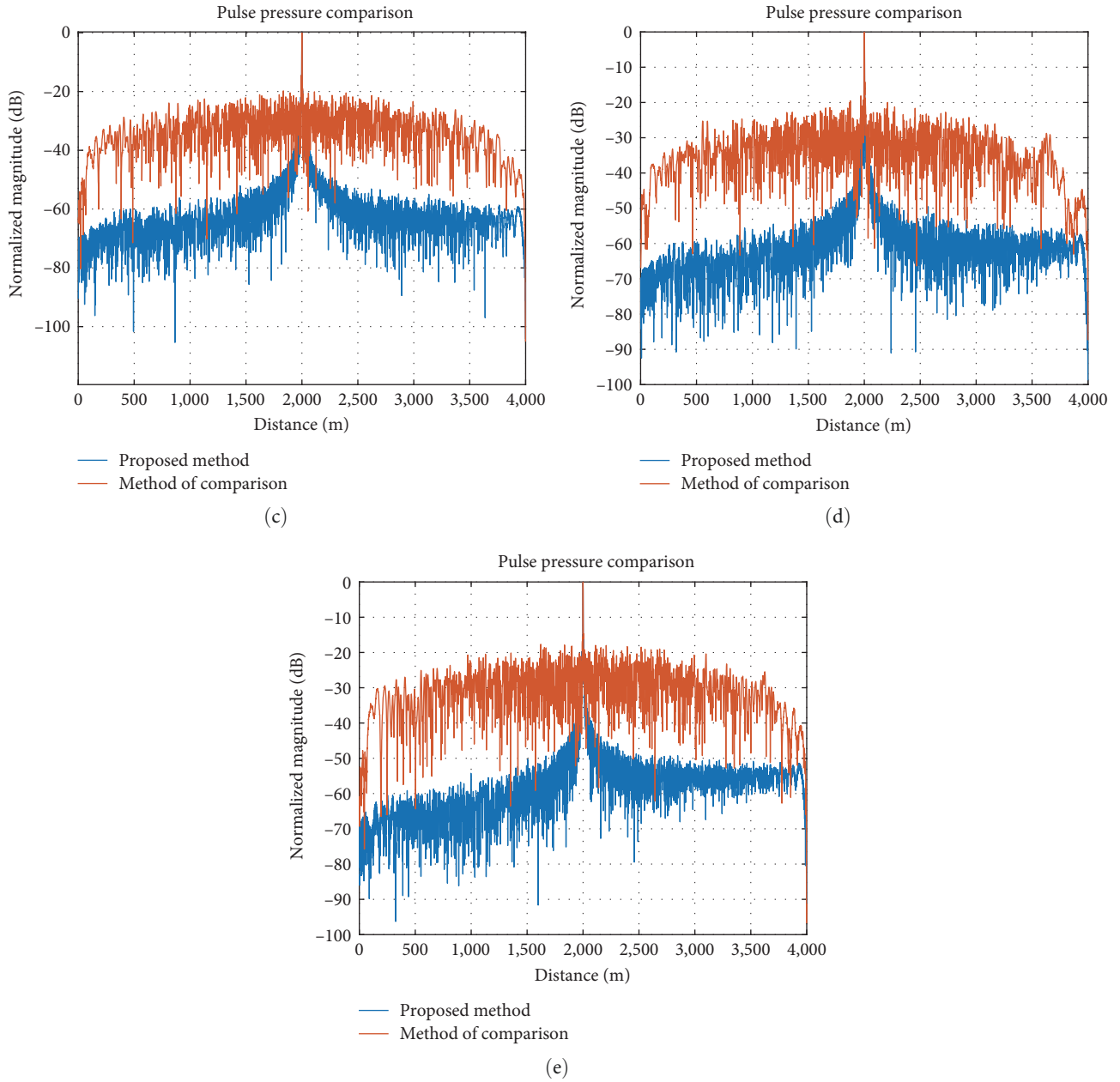

(a)

(b)

FIGURE 21: Continued.

FIGURE 21: Comparison of pulse pressure results between two algorithms for (a) ISRJ, (b) SMSP jamming, (c) C&I jamming, (d) smart noise convolution jamming, and (e) smart noise product jamming.

To enhance the clarity of our proposed algorithm's performance, we have incorporated additional experiments that involve other methods utilizing deep learning for jamming cancelation. In this expanded analysis, we compare our approach to another experiment in this manuscript. This added set of comparison experiments also applies DNNs to distinguish and eliminate jamming by considering distinct RF features in radar and jamming signals. However, the fundamental distinction lies in the design of the DNN responsible for extracting these RF features. Moreover, we extracted the RF features by designing two SSAEs, whereas the comparison experiment only extracted the RF features using a single conventional SSAE. Furthermore, the number of network layers

and node settings of the comparison algorithm are consistent with our proposed algorithm. However, the signals acquired by the experiment contain both RF and signal features. Consequently, if a single network is employed to extract the features, it will generate the two parts of the features that must be mixed together. This may not guarantee that the extracted RF features are better. Moreover, as the core idea of this paper consists of using the RF features of radar and jamming signals to differentiate, the performance of RF feature extraction can directly influence the performance of jamming suppression. Therefore, in these comparative experiments, a single self-encoder network is employed to initially extract the RF features. The subsequent jamming suppression process aligns
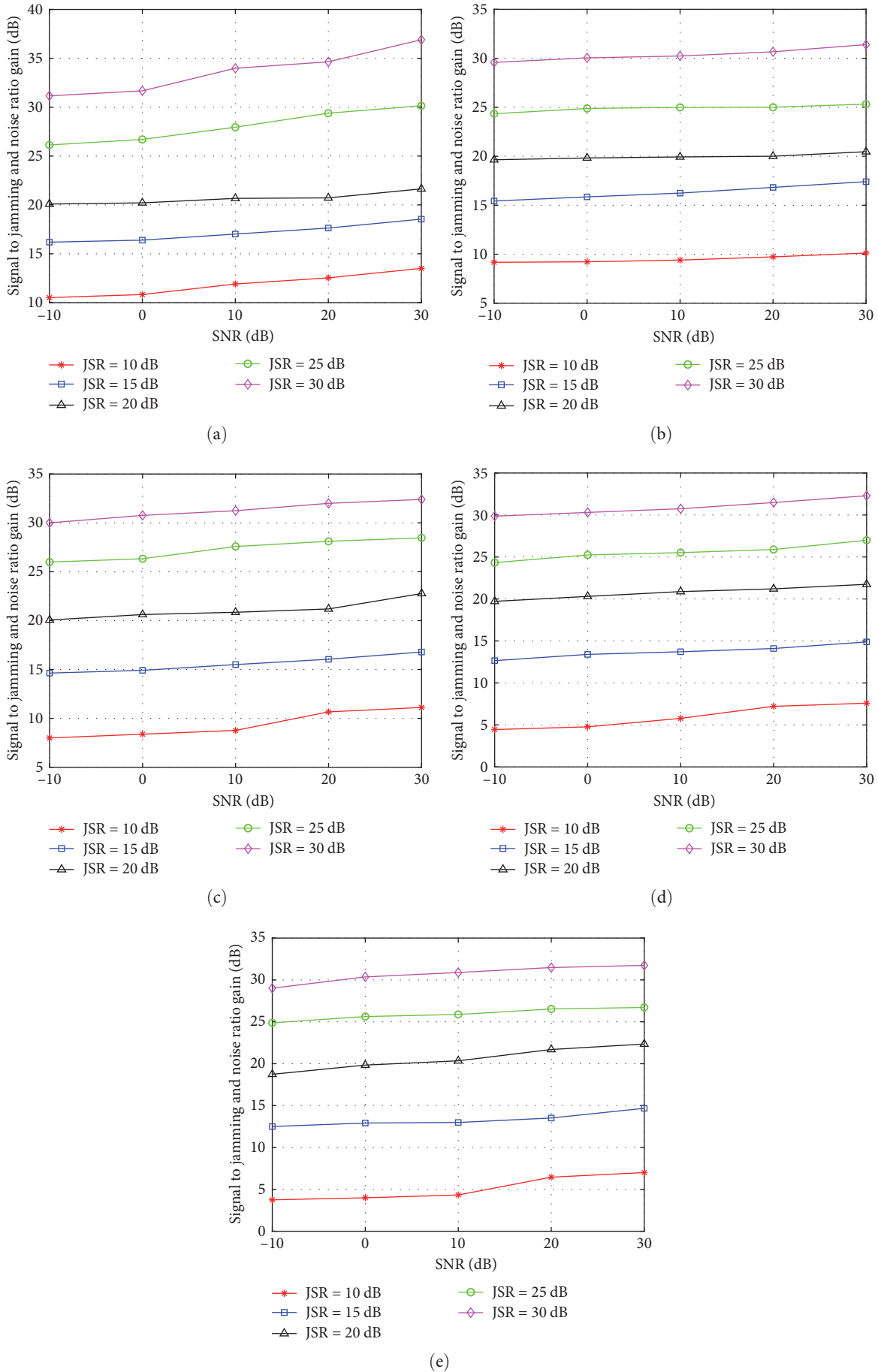
FIGURE 22: SINR gain after jamming suppression of comparison method for (a) ISRJ, (b) SMSP jamming, (c) C&I jamming, (d) smart noise convolution jamming, and (e) smart noise product jamming.

TABLE 5: Signal-to-jamming-to-noise ratio gain comparison.

Units (dB)	ISRJ	SMSP jamming	C&I jamming	Smart noise convolution jamming	Smart noise product jamming
Proposed method	50.6	49.0	46.8	38.3	44.3
Method of comparison	33.9	30.2	31.2	30.7	31.5

TABLE 6: Pulse compression comparison.

Units (dB)	ISRJ	SMSP jamming	C&I jamming	Smart noise convolution jamming	Smart noise product jamming
Proposed method	60.1	58.8	63.5	62.8	59.5
Method of comparison	20.8	18.5	21.3	25.4	23.7

with the methodology outlined in this paper. It involves using the extracted RF features as a label to constrain the mixed signal after JSAE coding hybrid features. Finally, the radar signal is reconstructed.

Figure 21(a)–21(e) shows the pulse compression comparison diagram after applying the jamming suppression between the comparative experiment and the proposed algorithm in this work. Each parameter of the signal, the signal-to-noise ratio, and the jamming-to-signal ratio are consistent with Figures 14–18. Furthermore, Figure 22(a)–22(e) shows the signal-to-jamming and noise ratio gain obtained after applying the jamming suppression in the comparative experiment. The comparison of the pulse pressure results of the two algorithms after eliminating jamming yields to confirm that the proposed algorithm generates obvious side lobe gain after pulse pressure compression. In addition, the discrepancy between the side lobes and the peak pulse pressure, following jamming suppression by the proposed algorithm, remains at −60 dB. The difference between the side lobe and the pulse pressure peak is obtained by applying a comparison algorithm after the jamming suppression and it is around 30 dB. Therefore, the pulse pressure results obtained by the proposed algorithm after the application of the suppressing jamming are closer to those without jamming, verifying that this algorithm is able to eliminate jamming more thoroughly. Furthermore, by comparing both algorithms in conjunction with Figures 19 and 22, it can be seen that the proposed algorithm can obviously generate a higher signal-to-jamming and noise ratio gain while using identical text jamming type, signal-to-noise ratio, and jamming-to-signal ratio. Moreover, according to the comparison algorithm, we have proposed a method where, as the signal-to-noise ratio increases, the gain in signal-to-jamming-to-noise ratio becomes more noticeable. Based on the comparison of the above two parts, the proposed algorithm has better jamming suppression performance. Finally, the comparison of jamming suppression performance also demonstrates the advantages of both SSAEs that were designed in this work to better extract the RF features.

Tables 5 and 6 present a comparison of the jamming suppression performance of the two algorithms, respectively. In more detail, Table 5 assesses the signal-to-jamming-to-noise ratio gain achieved after jamming suppression. Meanwhile, Table 6 evaluates the power difference between the target peak and side lobes obtained through pulse compression after

jamming suppression. To better simulate real-word situation, the background conditions applied for comparison represent a dry signal-to-noise ratio of 30 dB and a signal-to-noise ratio of 10 dB. The greater the difference between the target peak and the side lobe after pulse compression, the more helpful it is to accurately detect the target position.

6. Conclusion

We proposed a JSAE network to suppress several jamming types. The proposed method is based on the RF characteristics, which depend on the hardware and can be used to differentiate jamming signals from radar signals. Moreover, the RF characteristics of the radar signal are extracted using two SSAEs, and the JSAE filters out the jamming signal and reconstructs the radar signal to achieve jamming suppression. Moreover, the experimental results show that the JSAE could effectively filter out the jamming signal, facilitating the target detection and positioning after jamming suppression. The method of this paper exhibited better jamming suppression performance and generalization ability and higher efficiency than the traditional jamming suppression method even when varying the interference types. It does not require the estimation of the jamming parameters. In addition, the JSAE proved to be insensitive to noise. The proposed method generates pulse pressure peaks that are overlapped with the nonjamming signal for false target jamming and smart noise jamming, providing a high SINR gain at a low SNR, demonstrating its robustness.

Data Availability

The radar and jamming signals data used to support the findings of this study were supplied by Yaozu Yang under license and so cannot be made freely available. Requests for access to these data should be made to Yaozu Yang (yangyaozu@hrbeu.edu.cn).

Conflicts of Interest

The authors declare that they have no conflicts of interest.

Acknowledgments

References

[1] D. Feng, L. Xu, X. Pan, and X. Wang, "Jamming wideband radar using interrupted-sampling repeater," *IEEE Transactions on Aerospace and Electronic Systems*, vol. 53, no. 3, pp. 1341–1354, 2017.

[2] X. Wang, J. Liu, W. Zhang, Q. Fu, Z. Liu, and X. Xie, "Mathematic principles of interrupted-sampling repeater jamming (ISRJ)," *Science in China Series F: Information Sciences*, vol. 50, pp. 113–123, 2007.

[3] L. Lu and M. Gao, "An improved sliding matched filter method for interrupted sampling repeater jamming suppression based on jamming reconstruction," *IEEE Sensors Journal*, vol. 22, no. 10, pp. 9675–9684, 2022.

[4] S. Guo, J. Wang, G. Chen, and J. Wang, "Mainlobe interference suppression based on independent component analysis in passive bistatic radar," *IET Signal Processing*, vol. 12, no. 9, pp. 1193–1201, 2018.

[5] F. Cao, Z. Chen, X. Feng, C. He, and J. Xu, "Optimal design of anti-interrupted sampling repeater jamming waveform for missile-borne radar based on an improved genetic algorithm," *IET Signal Processing*, vol. 15, no. 9, pp. 622–632, 2021.

[6] Q. Lv, Y. Quan, M. Sha, W. Feng, and M. Xing, "Deep neural network-based interrupted sampling deceptive jamming countermeasure method," *IEEE Journal of Selected Topics in Applied Earth Observations and Remote Sensing*, vol. 15, pp. 9073–9085, 2022.

[7] S. Baher Safa Hanbali, "Countering self-protection smeared spectrum jamming against chirp radars," *IET Radar, Sonar & Navigation*, vol. 15, no. 4, pp. 382–389, 2021.

[8] S. Zhao, L. Zhang, Y. Zhou, and N. Liu, "Signal fusion-based algorithms to discriminate between radar targets and deception jamming in distributed multiple-radar architectures," *IEEE Sensors Journal*, vol. 15, no. 11, pp. 6697–6706, 2015.

[9] S. Zhao, L. Zhang, Y. Zhou, N. Liu, and J. Liu, "Discrimination of active false targets in multistatic radar using spatial scattering properties," *IET Radar, Sonar & Navigation*, vol. 10, no. 5, pp. 817–826, 2016.

[10] D. Huang, G. Cui, X. Yu, M. Ge, and L. Kong, "Joint range–velocity deception jamming suppression for SIMO radar," *IET Radar, Sonar & Navigation*, vol. 13, no. 1, pp. 113–122, 2019.

[11] G. Nie, G. Liao, C. Zeng, X. Zhang, and D. Li, "Joint radio frequency interference and deceptive jamming suppression method for single-channel SAR via subpulse coding," *IEEE Journal of Selected Topics in Applied Earth Observations and Remote Sensing*, vol. 16, pp. 787–798, 2023.

[12] D. Tian, W. Ren, L. Zhang, Z. Liang, and Q. Liu, "An adaptive scheme for chopping and interleaving jamming suppression based on the mismatched filter," in *2021 International Conference on Control, Automation and Information Sciences (ICCAIS)*, pp. 78–83, IEEE, Xi'an, China, October 2021.

[13] X. Li, C. Wang, H. Yuan, and S. Jin, "SMSP jamming suppression method based on jamming reconstruction and kurtosis maximum," *Journal of Beijing University of Aeronautics and Astronautics*, vol. 44, no. 6, pp. 1176–1184, 2018.

[14] G. Gok, Y. K. Alp, and O. Arikan, "A new method for specific emitter identification with results on real radar measurements," *IEEE Transactions on Information Forensics and Security*, vol. 15, pp. 3335–3346, 2020.

[15] O. Sevimli, A. E. Parker, A. P. Fattorini, and S. J. Mahon, "Measurement and modeling of thermal behavior in InGaP/GaAs HBTs," *IEEE Transactions on Electron Devices*, vol. 60, no. 5, pp. 1632–1639, 2013.

[16] G. Shi, Y. He, and C. Zhang, "Feature extraction and classification of cataluminescence images based on sparse coding convolutional neural networks," *IEEE Transactions on Instrumentation and Measurement*, vol. 70, pp. 1–11, 2021.

[17] J. Xie, Z. Li, Z. Zhou, and S. Liu, "A novel bearing fault classification method based on XGBoost: the fusion of deep learning-based features and empirical features," *IEEE Transactions on Instrumentation and Measurement*, vol. 70, pp. 1–9, 2021.

[18] X. Jiang, Y. Zhang, W. Zhang, and X. Xiao, "A novel sparse auto-encoder for deep unsupervised learning," in *2013 Sixth International Conference on Advanced Computational Intelligence (ICACI)*, pp. 256–261, IEEE, Hangzhou, China, October 2013.

[19] Q. V. Le, "Building high-level features using large scale unsupervised learning," in *2013 IEEE International Conference on Acoustics, Speech and Signal Processing*, pp. 8595–8598, IEEE, Vancouver, BC, Canada, May 2013.

[20] J. Deng, Z. Zhang, E. Marchi, and B. Schuller, "Sparse autoencoder-based feature transfer learning for speech emotion recognition," in *2013 Humaine Association Conference on Affective Computing and Intelligent Interaction*, pp. 511–516, IEEE, Geneva, Switzerland, September 2013.

[21] A. Sankaran, M. Vatsa, R. Singh, and A. Majumdar, "Group sparse autoencoder," *Image and Vision Computing*, vol. 60, pp. 64–74, 2017.

[22] J.-W. Shin, K.-H. Song, K.-S. Yoon, and H.-N. Kim, "Weak radar signal detection based on variable band selection," *IEEE Transactions on Aerospace and Electronic Systems*, vol. 52, no. 4, pp. 1743–1755, 2016.

[23] L. Zhang, W. Ma, and D. Zhang, "Stacked sparse autoencoder in PolSAR data classification using local spatial information," *IEEE Geoscience and Remote Sensing Letters*, vol. 13, no. 9, pp. 1359–1363, 2016.

[24] Y. Meng, L. Yu, Y. Wei, and P. Tong, "A novel parameter estimation method of interrupted sampling repeater jamming," in *2019 IEEE International Conference on Signal, Information and Data Processing (ICSIDP)*, pp. 1–5, IEEE, Chongqing, China, December 2019.

[25] Sparrow, M. Joseph, and J. Cikalo, "ECM techniques to counter pulse compression radar," US Patent 7,081,846, 2006.

[26] L. Zeng, H. Chen, Z. Zhang, W. Liu, Y. Wang, and L. Ni, "Cutting compensation in the time-frequency domain for smeared spectrum jamming suppression," *Electronics*, vol. 11, no. 13, Article ID 1970, 2022.

[27] L. Zhang, G. Wang, X. Zhang, and S. Li, "Smeared spectrum jamming suppression algorithm based on multiple orders 2D-FRFT," *Acta Armamentarii*, vol. 41, no. 9, pp. 1826–1836.

[28] Z. Liu, F. Dong, Y. Luo, Q. Zhang, K. Li, and D. Wang, "A suppression method against C&I jamming by time-frequency shift recombination," in *2021 International Conference on Control, Automation and Information Sciences (ICCAIS)*, pp. 280–285, IEEE, Xi'an, China, October 2021.

[29] Z. Liu, Q. Zhang, and K. Li, "A smart noise jamming suppression method based on atomic dictionary parameter optimization decomposition," *Remote Sensing*, vol. 14, no. 8, Article ID 1921, 2022.

[30] Y. Zhang, "Technology of smart noise jamming based on multiplication modulation," in *2011 International Conference on Electric Information and Control Engineering*, pp. 4557–4559, IEEE, Wuhan, China, April 2011.

[31] B. Han, X. Yang, X. Wu, and S. Li, "Smart noise jamming suppression method based on fast fractional filtering," *The Journal of Engineering*, vol. 2019, no. 19, pp. 6201–6205, 2019.